

# Measuring association with recursive rank binning

Chris Salahub<sup>1</sup> and Wayne Oldford<sup>1</sup>

<sup>1</sup>Department of Statistics and Actuarial Science, University of Waterloo

<sup>1</sup>{chris.salahub, rwoldford}@uwaterloo.ca

November 16, 2023

## Abstract

Pairwise measures of dependence are a common tool to map data in the early stages of analysis with several modern examples such as those in [Reshef et al. \(2011\)](#) and [Heller et al. \(2016\)](#) based on maximized partitions of the pairwise sample space. Following a short survey of modern measures of dependence, we introduce a new measure which recursively splits the ranks of a pair of variables to partition the sample space and computes the  $\chi^2$  statistic on the resulting bins. Splitting logic is detailed for splits maximizing a score function and randomly selected splits. Simulations indicate that random splitting produces a statistic conservatively approximated by the  $\chi^2$  distribution without a loss of power to detect numerous different data patterns compared to maximized binning. Though it seems to add no power to detect dependence, maximized recursive binning is shown to produce a natural visualization of the data and the measure. Applying maximized recursive rank binning to S&P 500 constituent data suggests the automatic detection of tail dependence.

## 1 Introduction

The modern world is awash with data. Ubiquitous data collection renders data sets comprised of ever more variables and observations which must be sifted through for insight. This is true, for example, in finance and genetics, where real time measurement and the advent of complete sequencing have resulted in truly massive raw data. In finance, the

identification of interesting pairwise variable relationships can motivate strategy or hedge risk, while the comparison of many genetic markers to a physical trait confers greater understanding of inheritance and the nature of some disease. How “interestingness” is measured in these and many other applications takes many different forms, such as the scagnostics of [Wilkinson et al. \(2005\)](#).

Perhaps the most widely used measure of interestingness is statistical dependence. A broad measure of the interestingness of a relationship between variables, it is defined as the absence of statistical independence and so includes a wide array of patterns. Consequently, many different measures devised for specific contexts and patterns of interest have been developed (e.g. [Goodman and Kruskal, 1979](#); [Liebetrau, 1983](#); [Choi et al., 2010](#); [Tjøstheim et al., 2022](#)) since the early efforts of Galton and Pearson to characterize it with correlation and the  $\chi^2$  test ([Stigler, 1989](#); [Hald, 1998](#)).

The eminence of statistical dependence is driven by the observation that it is almost universally interesting in an exploratory context. When sifting through many variable pairs to select those worthy of further investigation, a statistical dependency in a pair provides information about how the two variables should be controlled or modelled in any investigation.

The rise of computers has changed the nature of these proposals drastically, resulting in more flexible and computationally complex measures than ever before. Many modern measures of dependence are products of the computer age, such as algorithmic ones based on nearest neighbours ([Dümcke et al., 2014](#)), prediction ([Breiman, 2001](#)), or the maximization of a particular data transformation ([Breiman and Friedman, 1985](#); [Reshef et al., 2011](#); [Jiang et al., 2015](#); [Liu et al., 2018](#)).

A common feature of many measures of statistical dependence is the evaluation of functionals that compare the observed joint density to the product of marginal densities, as these address the problem of dependence directly using its definition.<sup>1</sup> In particular, much recent work has addressed *bin-based* methods which partition the pairwise sample space, as these automatically perform non-parametric estimation of the joint and product marginal densities ([Reshef et al., 2011](#); [Heller et al., 2016](#); [Cao et al., 2021](#)).

This work introduces and investigates a new measure of dependence based on a recursive partitioning, as in [Rahman \(2018\)](#). Section 2 outlines some necessary notation and defines

---

<sup>1</sup>The organization here is therefore somewhat different than is typical. Many works such as [Tjøstheim et al. \(2022\)](#), an up-to-date survey of measures of dependence, separate measures based on copulas, kernel functions, and partitioning. These are all cast here as particular instances of functionals comparing the joint and product marginal densities to emphasize similarities in the computation of these conceptually different measures in practice.

terms used in Section 3 to introduce a brief summary of measures of interestingness and dependence. Section 4 follows this general outline by focusing on bin-based measures of dependence and outlining previous proposals in a common notation.

The details of a new recursive partitioning method to measure association are described in Section 5, including a proofs that the coordinates of maximizing splits occur at observations and a discussion of stop criteria and general splitting logic. All of this is combined in the pseudo-code algorithms of Section 6 before the details of a package implementing the method in R are discussed in Section 7. Simulations carried out in Section 8 characterize the null distribution of the algorithm for different sample sizes and indicate that recursive binning powerfully detects many different patterns of dependence, even when the split choice is made randomly. Finally, the algorithm is applied to S&P 500 constituent data in Section 9 with results that suggest maximized splits detect patterns of specific interest such as tail dependence automatically.

## 2 Preliminaries

Let  $X$  and  $Y$  be a pair of random variables with distribution functions  $F_X(x)$  and  $F_Y(y)$  over the domains  $\mathcal{X}$  and  $\mathcal{Y}$  both respectively. Denote the joint distribution of the pair  $X, Y$  as  $F_{X,Y}(x, y)$ , and the conditional distributions  $F_{X|Y}(x|y)$  and  $F_{Y|X}(y|x)$ . To remain fully general, note that both of  $X$  and  $Y$  may be continuous or discrete. Let  $f_X(x)$ ,  $f_Y(y)$ ,  $f_{X,Y}(x, y)$ ,  $f_{X|Y}(x|y)$ , and  $f_{Y|X}(y|x)$  be the corresponding probability densities or probability mass functions in the continuous or discrete cases. We say that  $X$  and  $Y$  are independent and write  $X \perp\!\!\!\perp Y$  if and only if

$$f_{X,Y}(x, y) = f_X(x)f_Y(y) \tag{1}$$

or equivalently  $f_{X|Y}(x|y) = f_X(x)$  and  $f_{Y|X}(y|x) = f_Y(y)$ .

Define a  $K$ -dimensional copula as a distribution function  $C(u_1, u_2, \dots, u_K)$  over  $[0, 1]^k$  with uniform marginal distributions for all  $u_k$  as in Embrechts et al. (2001). By Sklar's Theorem, for any  $K$  continuous random variables there exists a unique copula  $C$  such that

$$F_{X_1, X_2, \dots, X_K}(x_1, x_2, \dots, x_K) = C(F_{X_1}(x_1), F_{X_2}(x_2), \dots, F_{X_K}(x_K)), \tag{2}$$

that is the joint distribution can be summarized by a copula on the marginals transformed to be uniformly distributed. In other words: the relationship between the variables is uniquely determined by  $C$  and the marginals alone. Define the independence copula

$$C_I(u_1, u_2, \dots, u_K) = \prod_{k=1}^K u_k. \tag{3}$$

In particular, consider the copula of  $X$  and  $Y$ ,  $C(F_X(x), F_Y(y)) = C(u, v)$ , and the bivariate independence copula,  $C_I(u, v) = uv$ .

In practice these theoretical quantities are unknown. Instead, all that is available is a sample of paired observations  $(x_1, y_1), (x_2, y_2), \dots, (x_n, y_n)$  of  $(X, Y)$ . Let  $\mathbf{x} = (x_1, x_2, \dots, x_n)^\top$  and  $\mathbf{y} = (y_1, y_2, \dots, y_n)^\top$  be the observed values of  $X$  and  $Y$  respectively. For  $X$  and  $Y$  which can be ordered, let a subscript  $(x)$  indicate a non-decreasing sorting of elements with respect to  $\mathbf{x}$  so that  $\mathbf{x}_{(x)}$  is the vector  $\mathbf{x}$  in increasing order and  $\mathbf{y}_{(x)}$  is the vector  $\mathbf{y}$  sorted in increasing order of  $\mathbf{x}$ . Elementwise, follow the convention

$$\mathbf{x}_{(x)} = (x_{(1)}, x_{(2)}, \dots, x_{(n)})^\top$$

to denote the elements of  $\mathbf{x}_{(x)}$  and analogously for  $\mathbf{y}_{(y)}$ . Define the rank function on a marginal sample  $\mathbf{x}$  as

$$r(x; \mathbf{x}) = \sum_{i=1}^n I_{(-\infty, x]}(x_i), \quad (4)$$

where

$$I_A(x) = \begin{cases} 1 & \text{if } x \in A \\ 0 & \text{otherwise} \end{cases}$$

is the usual indicator function so that  $r(x_i; \mathbf{x})$  gives the index of  $x_i$  in  $\mathbf{x}_{(x)}$ . Note that this definition assumes  $x_i \neq x_j$  for all  $i \neq j$ , the case of no *ties*.

To consider different conventions to address ties, suppose  $x_1 = x_2 = \dots = x_m = x_{(1)}$  for  $m < n$ . In this case,  $r(x_1; \mathbf{x}) = r(x_2; \mathbf{x}) = \dots = r(x_m; \mathbf{x}) = m$ , that is all are given the *maximum* index  $m$ . It is not clear this must be the case, as choosing the *minimum* index 1 seems equally valid for these first  $m$  observations. Another option is *random tie-breaking*, which randomly assigns the indices  $1, 2, \dots, m$  to  $x_1, x_2, \dots, x_m$ . Random tie breaking is of particular interest, as it induces a uniform distribution on the ranks for tied regions. For applications where complete ranks are necessary, this is more desirable than the gaps introduced by the maximum or minimum indexing.

We can then define the empirical distribution function for these ordered cases as

$$\widehat{F}_{\mathbf{x}}(x) = \frac{1}{n} r(x; \mathbf{x}) = \frac{1}{n} \sum_{i=1}^n I_{(-\infty, x]}(x_i), \quad (5)$$

with  $\widehat{F}_{\mathbf{y}}(y)$  defined similarly. The empirical copula of  $X$  and  $Y$  is defined as

$$\widehat{C}(u, v) = \frac{1}{n} \sum_{i=1}^n I_{(-\infty, u]} \left( \frac{r(x_i; \mathbf{x})}{n} \right) I_{(-\infty, v]} \left( \frac{r(y_i; \mathbf{y})}{n} \right). \quad (6)$$

Finally, define the vector-valued rank function as

$$\mathbf{r}(\mathbf{x}) = (r(x_1; \mathbf{x}), r(x_2; \mathbf{x}), \dots, r(x_n; \mathbf{x}))^\top. \quad (7)$$

For discrete  $X$  without ordered values, take an arbitrary numbering of the possible values in  $\mathcal{X}$  and let  $I = |\mathcal{X}|$ . Otherwise, number such that the assigned values reflect the ordering. If  $Y$  is discrete, number  $\mathcal{Y}$  similarly with  $J = |\mathcal{Y}|$ . Then, for  $\mathbf{x}$  and  $\mathbf{y}$ , define the observed marginal and joint counts

$$o_{i+} = \sum_{j=1}^J \sum_{k=1}^n I_{\{(i,j)\}}((x_k, y_k)) = \sum_{j=1}^J o_{ij} \quad (8)$$

and  $o_{+j}$  analogously. These give corresponding probability estimates  $\hat{p}_{ij}$ ,  $\hat{p}_{i+}$ , and  $\hat{p}_{+j}$  when divided by  $n$ .

Distinguish three different *types* of  $X$  and  $Y$  based on  $\mathcal{X}$  and  $\mathcal{Y}$ . The three types are:

**continuous** some interval or collection of intervals of real numbers;

**ordinal categorical** discrete possibilities with an ordering (e.g. income brackets);

**nominal categorical** discrete possibilities without an ordering (e.g. country of birth).

The possible combinations of these lead to six unique pairwise combinations. Following the convention of [Lee and Huh \(2003\)](#), call comparisons of data of the same type *simple* comparisons. *Complex* comparisons refer to the unique pairings between types: continuous versus ordinal, continuous versus nominal, and ordinal versus nominal.

Introduce the function

$$G : \mathcal{X} \times \mathcal{Y} \mapsto \mathcal{R}$$

quantifying some pattern of interest between  $X$  and  $Y$  with a value in  $\mathcal{R} \subset \mathbb{R}$ . For the purpose of this work, any such  $G$  is called a *measure of interestingness* or simply a *measure*. The term “interestingness” is used instead of “association” following the tradition of researchers such as John W. Tukey (see [Friedman and Stuetzle \(2002\)](#)) and to avoid the implications of “association”, typically used to describe *statistical dependence* as in Equation (1).

Consider, for example, Tukey’s scagnostic measures of *structure* as reintroduced in [Wilkinson et al. \(2005\)](#). Two different constructed data sets exemplifying the scagnostics for “stringiness” and “clumpiness” respectively are shown in Figure 1. Both of these

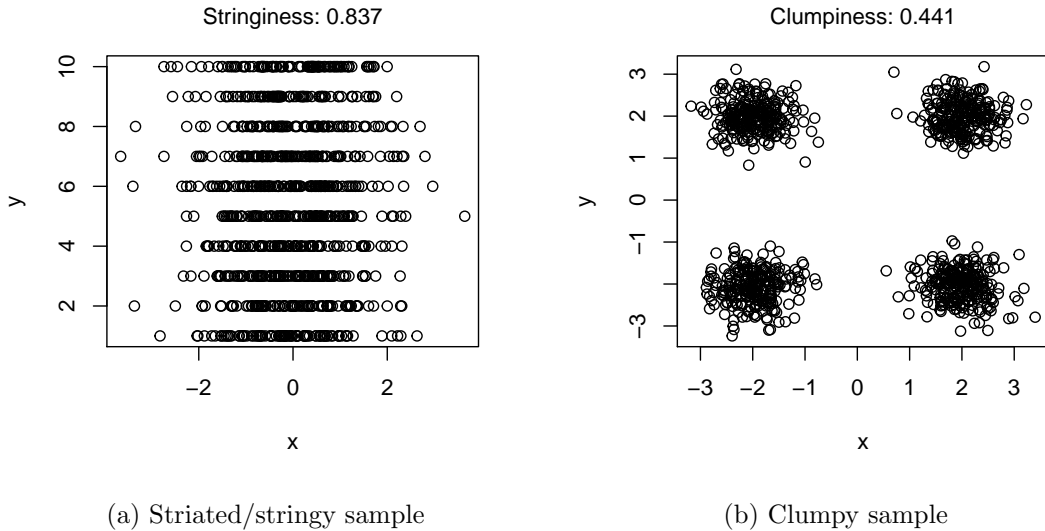


Figure 1: Data exhibiting certain scagnostic structures despite the independent generation of  $x$  and  $y$ .

simulated data sets have margins generated independently of each other, and still have relatively large values for their respective measures compared to the null distributions in [Wilkinson and Wills \(2008\)](#). While scagnostics have been expressly developed to capture patterns other than statistical independence, calling them measures of association confuses the term.<sup>2</sup> Another example is  $\lambda_b$  from [Goodman and Kruskal \(1979\)](#), which is motivated by prediction and not strictly tied to dependence.

Numerous frameworks have been proposed to evaluate candidates for  $G$ . A statistical framework is given in [Rényi \(1959\)](#), and this framework has been subsequently updated by [Schweizer and Wolff \(1981\)](#) and [Móri and Székely \(2019\)](#). [Reimherr and Nicolae \(2013\)](#) present a slightly different framework which emphasizes interpretability and delineates three different motivations for measuring association. Here, the focus is on the *ordering*  $G$  induces on  $\mathcal{X} \times \mathcal{Y}$ , as this can accomplish all of the goals from [Reimherr and Nicolae \(2013\)](#) and is critical to the search for interesting variables.

The importance of ordering restricts most measures of interestingness to a range on a

---

<sup>2</sup>See, for example [Liu et al. \(2018\)](#) utilizing data analogous to Figure 1(b) as an example of ‘association’ in a paper motivated by statistical independence.

finite interval  $\mathcal{R} = [g_{\min}, g_{\max}] \subset \mathbb{R}$ . The upper bound is obtained for  $X$  and  $Y$  exemplary of the pattern of interest, while  $g_{\min}$  is less consistent. For signed measures, such as Pearson’s correlation coefficient,  $g_{\min}$  may still indicate perfect correspondence to a particular pattern. In unsigned measures  $g_{\min}$  suggests no indication of the pattern<sup>3</sup>. The  $X$  and  $Y$  which lead to these extremes are typically not unique, but rather represent a family of patterns which the measure does not distinguish.

Commonly,  $G(X, Y)$  is scaled by  $\max\{|g_{\max}|, |g_{\min}|\}$  such that  $\mathcal{R}$  is restricted to  $[-1, 1]$  or  $[0, 1]$ . By scaling  $G$  by the magnitude of its most extreme value, the ordering it imposes is made explicit. For any pair  $X$  and  $Y$ , this scaled measure communicates directly how the pair compares to the perfect example. This scaling can be misleading, however, when the analyst is unfamiliar with its distribution along its range.

### 3 Measuring dependence

As noted by [Cramér \(1924\)](#); [Fairfield Smith \(1957\)](#); [Goodman and Kruskal \(1979\)](#) and likely others, measures are devised to capture specific patterns. This is often desirable for interpretability, as [Reimherr and Nicolae \(2013\)](#) note, and can lead to descriptive adjectives which evoke a measure, as in the scagnostics of [Wilkinson et al. \(2005\)](#). Some common patterns and corresponding measures are:

**linearity** which is typically measured by Pearson’s product moment correlation;

**monotonicity** captured by Spearman’s  $\rho$ , the rank version of correlation;

**concordance** measured by Kendall’s  $\tau$  and Goodman and Kruskal’s  $\gamma$  (from [Goodman and Kruskal \(1979\)](#));

**predictability** measured by Goodman and Kruskal’s  $\lambda$  (also from [Goodman and Kruskal \(1979\)](#));

**agreement** addressed by the  $\kappa$  measure of inter-rater reliability from [Cohen \(1960\)](#);

and others listed in [Liu et al. \(2018\)](#); [Liebetrau \(1983\)](#); [Agresti \(1981\)](#); and [Goodman and Kruskal \(1979\)](#).

---

<sup>3</sup>Any signed measure  $G$  can, of course, be made unsigned by taking  $|G|$ .

The variety of patterns which one might want to measure and the different types of  $X$  and  $Y$  have led to a great proliferation of bivariate measures of interestingness<sup>4</sup>, each with its own interpretation. Unfortunately, the division of measures by both type and pattern makes the search for interesting patterns in complex data far more challenging, with research such as [Khamis \(2008\)](#) and [Lee and Huh \(2003\)](#) devoted to the task of guiding practitioners to choose the most comparable measures between types. In practice, correlation is often applied to all variable pairs regardless of type, despite its well-known shortcomings as outlined in [Tjøstheim et al. \(2022\)](#); [Reshef et al. \(2011\)](#); and [Anscombe \(1973\)](#).

Regardless of motivation or type, however,  $X$  and  $Y$  satisfying Equation (1) are universally considered uninteresting. As a consequence, complex measures of interestingness typically attempt to measure departures from statistical independence. These measures of statistical dependence are functionals of the form

$$D(f_{X,Y}(x, y), f_X(x)f_Y(y)) \quad (9)$$

which compare the joint and marginal product distributions of  $X$  and  $Y$ . Often, they will attempt to satisfy the desiderata outlined by [Rényi \(1959\)](#) or [Schweizer and Wolff \(1981\)](#), the latter of which relaxed the axioms of the former after noting they are unnecessarily restrictive and hard to apply in practice. Some examples for continuous  $X$  and  $Y$  include

$$\Delta(X, Y) = \int \int_{\{(x,y): f_{X,Y}(x,y) \geq f_X(x)f_Y(y)\}} [f_{X,Y}(x, y) - f_X(x)f_Y(y)] dx dy \quad (10)$$

from [Silvey \(1964\)](#) and mutual information

$$\mathcal{I}(X, Y) = D_{KL}(f_{X,Y} || f_X f_Y) = \int_{\mathcal{Y}} \int_{\mathcal{X}} f_{X,Y}(x, y) \log \left( \frac{f_{X,Y}(x, y)}{f_X(x)f_Y(y)} \right) dx dy \quad (11)$$

from [Shannon \(1948\)](#), where  $D_{KL}(F || G)$  denotes the Kullback-Leibler divergence of  $G$  from  $F$ . For discrete  $X$  and  $Y$  a classic example is the  $\chi^2$  statistic for independence from [Pearson \(1900\)](#)<sup>5</sup>

$$\mathcal{D}(X, Y) \propto \sum_{x \in \mathcal{X}} \sum_{y \in \mathcal{Y}} \frac{[f_{X,Y}(x, y) - f_X(x)f_Y(y)]^2}{f_X(x)f_Y(y)}. \quad (12)$$

---

<sup>4</sup>The  $2 \times 2$  contingency table, for example, has an almost overwhelming roster of measures analyzed in [Choi et al. \(2010\)](#).

<sup>5</sup>Note that this formulation of  $\mathcal{D}(X, Y)$  is somewhat atypical, as this is a quantity usually defined on the sample  $\mathbf{x}, \mathbf{y}$ .



Another possible functional based on the cumulative distribution functions is given by [Hoeffding \(1948\)](#)

$$D_H(X, Y) = \int (F(x, y) - F(x, \infty)F(\infty, y))^2 dF(x, y). \quad (13)$$

Central to all of these measures is the factorization definition of independence from Equation (1). In every case, some comparison is made between  $f_{X,Y}(x, y)$  and  $f_X(x)f_Y(y)$  which is zero when the two are equal almost everywhere.

For any function of the form in Equation (9), an equivalent measure exists in the copula space. By Sklar’s Theorem, discussed in [Sklar \(1996\)](#) and summarized in [Embrechts et al. \(2001\)](#), the dependence between  $X$  and  $Y$  can be captured by the marginal distribution functions  $F_X$  and  $F_Y$  and their copula  $C$ . Just as in Equation (1),  $X$  and  $Y$  are independent only if their copula is the independence copula  $C_I(u, v) = uv$ . [Schweizer and Wolff \(1981\)](#) therefore show that a transform can be applied to any measure formulated in  $F_X(x)$ ,  $F_Y(y)$ , and  $F_{X,Y}(x, y)$  to convert it to a functional of the form

$$D^*(C(F_X(u), F_Y(v)), uv).$$

Such transforms are attractive because they remove the marginal distributions of the variables being compared. This allows for non-parametric estimation of quantities without presuming any particular distribution. Indeed, there are many proposed measures which utilize empirical copulas, such as those presented in [Ding et al. \(2017\)](#); [Siburg and Stoimenov \(2010\)](#); and [Genest and Rémillard \(2004\)](#).

Measures like the distance covariance of [Székely and Rizzo \(2009\)](#) instead apply a functional of the form in Equation (9) to the characteristic functions of  $X$  and  $Y$ . The characteristic function of  $X$  is defined as

$$\phi_X(t) = E[e^{itX}], \quad (14)$$

where  $E$  is the expectation operator with respect to  $X$ . The joint characteristic function,  $\phi_{X,Y}(t, s)$ , and characteristic function of  $Y$ ,  $\phi_Y(s)$ , are defined similarly. This is based on an important result of Equation (1), that  $\phi_{X,Y}(s, t) = \phi_X(t)\phi_Y(s)$  if and only if  $X \perp\!\!\!\perp Y$ .

Equation (9) is really just an evaluation of the goodness of fit of  $f_X(x)f_Y(y)$  to  $f_{X,Y}(x, y)$ , and this creates an obvious analogy to empirical distribution function goodness of fit tests as described in [Zheng et al. \(2021\)](#) and [Stephens \(1974\)](#). Many common measures of functional distance appear in the literature of independence tests, such as the Kolmogorov-Smirnov test in [Heller et al. \(2016\)](#) and results for any  $L_P$  distance in [Schweizer and Wolff](#)

(1981). These can be made even more general by replacing Euclidean distances by kernel distances, as in Liu et al. (2018) or the Hilbert-Schmit independence criterion (HSIC) of Gretton et al. (2007). While Liu et al. (2018) maximize over a pre-specified set of kernel distances, Lopez-Paz et al. (2013) instead introduce a measure which randomly transforms  $X$  and  $Y$  and takes the maximum of the applied random transforms.

More unique applications of goodness of fit principles are found in Dümcke et al. (2014) and Heller et al. (2013). Dümcke et al. (2014) utilize the exact distribution of nearest neighbour distances under independence to develop two novel tests. Rather than comparing the joint distribution to a product of marginals, their tests are based on the deviation between the exact distribution of nearest neighbours and that observed in a sample. Heller et al. (2013) make use of local distances about each point in turn to construct a series of contingency tables and then aggregate the  $p$ -values gained.

The generation of numerous tables evokes a relevant class of measures based on the application of measures as in Equation (9) to partitions of the outcome space  $\mathcal{X} \times \mathcal{Y}$ , after which the values are aggregated. Such partitioning essentially allows for local estimation of  $f_{X,Y}$  and  $f_X f_Y$  without a parametric family. Rather, the estimate relies only on the choice of partition. Another benefit of such partitioning is it permits the application of the same test to any data type, as partitioning continuous data produces ordinal categorical data. As a consequence of this potential and their popularity in recent literature, this work primarily focuses on these methods.

## 4 Bin-based measures

Though it has become more popular as it has become computationally feasible, partitioning, or *binning*, has always had a role in computing measures of association. See, for example, the early investigations into the  $\chi^2$  test outlined in Plackett (1983). Rather than using  $X$  and  $Y$  directly, a binning function can be applied to their marginal values in order to discretize them.<sup>6</sup> Therefore, discussing a measure which *induces* bins only makes sense when at least one of  $X$  and  $Y$  is continuous, though the results can be applied to categorical cases.

A univariate binning on  $J$  bins is a function  $b : \mathcal{B} \mapsto \{1, \dots, J\}$  which partitions its continuous domain  $\mathcal{B} \subseteq \mathbb{R}$  into  $J$  distinct parts, or *bins*. Any such  $b$  has a vector-valued

---

<sup>6</sup>In the case where one of  $X$  and  $Y$  is already categorical, this reduces to the  $K$ -sample problem. Some proposals, such as Heller et al. (2016), switch freely between this  $K$ -sample problem and the problem of measuring association.

version  $\mathbf{b} : \mathcal{B}^p \mapsto \{1, \dots, J\}^p$  such that  $\mathbf{b}(\mathbf{x}) = (b(x_1), \dots, b(x_n))^\top$  for  $\mathbf{x} \in \mathcal{B}^p$ . Consider applying  $b_X : \mathcal{X} \mapsto \{1, \dots, I\}$  to  $X$  and  $b_Y : \mathcal{Y} \mapsto \{1, \dots, J\}$  to  $Y$ . That is apply a binning on  $I$  bins to  $X$  and a binning on  $J$  bins to  $Y$ . This is equivalent to an  $I \times J$  grid on  $\mathcal{X} \times \mathcal{Y}$ , and so the bins can be indexed by  $(i, j)$  to correspond with the values  $(b_X(X), b_Y(Y))$ . Define

$$\epsilon_{ij} = n \int_{\{x: b_X(x)=i\}} dF_X(x) \int_{\{y: b_Y(y)=j\}} dF_Y(y), \quad (15)$$

the expected count of observations of  $n$  which fall into bin  $(i, j)$  under independence. Note that in the case of uniform  $X$  and  $Y$ , this simplifies to  $n$  times the area of the  $(i, j)$  bin.

In practice the vectors  $\mathbf{x}$  and  $\mathbf{y}$  are all that is observed, so define the analogous sample quantity

$$e_{ij} = \frac{1}{n} \sum_{k=1}^n I_{\{i\}}(b_X(x_k)) \sum_{l=1}^n I_{\{j\}}(b_Y(y_l)). \quad (16)$$

The observed  $(i, j)$  bin count is given by

$$o_{ij} = \sum_{k=1}^n I_{\{(i,j)\}}((b_X(x_k), b_Y(y_k))), \quad (17)$$

so  $e_{ij} = n \frac{o_{i+}}{n} \frac{o_{+j}}{n}$  using the notation of Equation (8). Under this binning,  $X$  and  $Y$  are converted to the contingency table in Table 1. Once so binned, the  $o_{ij}$  and  $e_{ij}$  can be used

	$b_Y(y) = 1$	$b_Y(y) = 2$	$\dots$	$b_Y(y) = J$	
$b_X(x) = 1$	$o_{11}$	$o_{12}$	$\dots$	$o_{1J}$	$o_{1+}$
$b_X(x) = 2$	$o_{21}$	$o_{22}$	$\dots$	$o_{2J}$	$o_{2+}$
$\vdots$	$\vdots$	$\vdots$	$\ddots$	$\vdots$	$\vdots$
$b_X(x) = I$	$o_{I1}$	$o_{I2}$	$\dots$	$o_{IJ}$	$o_{I+}$
	$o_{+1}$	$o_{+2}$	$\dots$	$o_{+J}$	$n$

Table 1: The contingency table imposed on  $\mathbf{x}$  and  $\mathbf{y}$  by the binnings  $b_X(x)$  applied to  $\mathbf{x}$  and  $b_Y(y)$  applied to  $\mathbf{y}$ .

to in place of the unknown densities in Equations (10), (11), and (12) nonparametrically. In this way, a grid is simply a particular kind of two-dimensional histogram.<sup>7</sup> For Silvey's

<sup>7</sup>There are many other possible tessellations which produce a two-dimensional histogram density estimate, see Carr et al. (1987) and Scott (1988)

$\Delta$  from Equation (10), the analogue on the binned data in Table 1 is

$$\Delta(\mathbf{b}_x, \mathbf{b}_y) = \sum_{\{(i,j):o_{ij} \geq e_{ij}\}} \sum_{\{(i,j):o_{ij} \geq \frac{1}{n}o_{i+}o_{+j}\}} \frac{o_{ij} - e_{ij}}{n} = \sum_{\{(i,j):o_{ij} \geq \frac{1}{n}o_{i+}o_{+j}\}} \sum_{\{(i,j):o_{ij} \geq \frac{1}{n}o_{i+}o_{+j}\}} \frac{no_{ij} - o_{i+}o_{+j}}{n^2}; \quad (18)$$

Shannon’s mutual information from Equation (11) becomes the multinomial log-likelihood ratio

$$\mathcal{I}(\mathbf{b}_x, \mathbf{b}_y) = \sum_{i=1}^I \sum_{j=1}^J \frac{o_{ij}}{n} \log \left( \frac{o_{ij}}{e_{ij}} \right) = \sum_{i=1}^I \sum_{j=1}^J \frac{o_{ij}}{n} \log \left( \frac{no_{ij}}{o_{i+}o_{+j}} \right); \quad (19)$$

and Pearson’s  $\chi^2$  measure from Equation (12) becomes

$$\mathcal{D}(\mathbf{b}_x, \mathbf{b}_y) = \sum_{i=1}^I \sum_{j=1}^J \frac{(o_{ij} - e_{ij})^2}{e_{ij}} = \frac{1}{n} \sum_{i=1}^I \sum_{j=1}^J \frac{(no_{ij} - o_{i+}o_{+j})^2}{o_{i+}o_{+j}}, \quad (20)$$

where  $\mathbf{b}_x = \mathbf{b}_X(\mathbf{x})$  and  $\mathbf{b}_y = \mathbf{b}_Y(\mathbf{y})$  are used for brevity. While  $\mathbf{b}_X$  and  $\mathbf{b}_Y$  can be arbitrarily defined, Equations (18), (19), and (20) depend only on the counts in each cell of Table 1. Therefore, only the values of  $\mathbf{x}$  and  $\mathbf{y}$  need to be considered as possible partition boundaries, or *bin edges*. Considering edges between every point, and not allowing for identical  $\mathbf{x}$  and  $\mathbf{y}$  values, this means are  $n - 1$  possible bin edges to consider in each of  $\mathbf{x}$  and  $\mathbf{y}$ . Noting that the bin edges can either be present or absent, there are therefore  $2^{n-1}2^{n-1} = 4^{n-1}$  possible contingency tables for a given  $\mathbf{x}$  and  $\mathbf{y}$ .

There is often no a priori exploratory reason to choose a particular binning, and so methods from Reshef et al. (2011); Jiang et al. (2015); Heller et al. (2016); and Reshef et al. (2018) have the exploration of this large number of grids at their core. Reshef et al. (2011) and Reshef et al. (2018), in the introduction of the maximal information criterion (MIC), propose computing Equation (19) for all grids such that  $IJ \leq n^{0.6}$ , scaling these values, and storing them in a matrix  $M$ . The maximal value of this matrix is then taken as the MIC.<sup>8</sup> In order to contextualize MIC values,  $p$ -values based on simulated null data sets are computed.

Jiang et al. (2015) propose a penalized version of Equation (19) to find a solution. The particular penalty is outlined in Equation (24). Conceptually this penalized optimization assumes a Poisson distribution on the number of bins for one of the margins conditioned

---

<sup>8</sup>It should be noted that even this space is too large to fully explore, and so only a small number of actual grids are computed by their algorithm in practice. Their concept of *equitability* has also generated considerable controversy. See the discussions in Gorfine et al. (2012); Kinney and Atwal (2014a); Reshef et al. (2014); Kinney and Atwal (2014b); and Simon and Tibshirani (2014).

on the other and then maximizes the likelihood using a dynamic algorithm. As with the MIC, the null distribution of this method is determined empirically.

Hoeffding (1948) restricts the exploration only to  $I = J = 2$ , and proposes a sum of Equation (13) for all unique possible two-by-two grids, which Thas and Ottoy (2004) show is asymptotically equivalent to Equation (20) evaluated over all two-by-two grids with a suitable scaling. Heller et al. (2016) extend this by simply restricting the grid to  $m$  divisions on both margins. They investigate both summation and maximization for either of Equation (20) and (19) across all possible  $m \times m$  grids. In the case of summation, the values over all possible  $m \times m$  grids are computed and the sum is returned, while the maximization case reports only the largest of these values. The distributions of these statistics is computed empirically just as for the MIC and Jiang et al. (2015). The language used, where aggregation is compared to the Cramer-von Mises criterion and maximization to the Kolmogorov-Smirnov test, is evocative of methods for testing empirical distribution functions in Stephens (1974).

To implement these methods, all of Heller et al. (2016); Jiang et al. (2015); and Reshef et al. (2011) utilize similar recursive algorithms. While Heller et al. (2016) compute their summation statistic directly, as this reduces to a counting problem, they borrow the procedure of Jiang et al. (2015) with a different penalty for the maximization case. Reshef et al. (2011) use a similar concept to guide their exploration of the space of grids with  $IJ \leq n^{0.6}$ .

For a more detailed discussion of this recursive algorithm and its applications, introduce the notation

$$D(\mathbf{b}_x, \mathbf{b}_y) = \sum_{i=1}^I \sum_{j=1}^J d(o_{ij}, e_{ij}), \quad (21)$$

thereby expressing  $D$  over the entire data set as the sum of  $d$  applied to each cell. Introduce the subscript notation

$$\mathbf{b}_{x[1:k]} = (b_X(x_1), b_X(x_2), \dots, b_X(x_k))^T$$

to denote a binning on  $I$  bins applied to the first  $k$  elements of  $\mathbf{x}$ . Consider the value of Equation (21) applied to the first  $k$  observations of  $\mathbf{x}$  and  $\mathbf{y}$  with a given binning on  $\mathbf{y}$ , written

$$D_k(\cdot | \mathbf{b}_y) : \{1, \dots, I\}^k \mapsto \mathbb{R} \quad (22)$$

for  $I \leq k$  and a given binning  $\mathbf{b}_y$  on  $J$  bins defined for all of  $\mathbf{y}$  (not just the first  $k$  observations).

Equation (22) presents an important modification of Equation (21). By viewing only the first  $k$  elements with a *pre-specified*  $\mathbf{b}_y$ , the problem of identifying a binning which

optimizes  $D_k$  is greatly simplified compared to  $D$ . Rather than selecting among all possible grids, only a small number at each step need to be considered. Suppose  $\mathbf{b}_{\mathbf{x}[1:k]}^*$  is the binning on the first  $k$  elements of  $\mathbf{x}$  which maximizes  $D_k$ , define

$$D_k^* = D_k(\mathbf{b}_{\mathbf{x}[1:k]}^* | \mathbf{b}_{\mathbf{y}}),$$

as the maximal value of Equation (22). It is therefore the maximal value of  $D$  applied to the first  $k$  observations of  $\mathbf{x}$  and  $\mathbf{y}$  given a known binning on  $\mathbf{y}$ .

Using this general notation, the recursive estimate  $\widehat{D}_k^*$  used by Reshef et al. (2011); Jiang et al. (2015); and Heller et al. (2016) is

$$\widehat{D}_k^* = \max_{1 \leq i < k} \left[ \widehat{D}_{i-1}^* + \sum_{j=1}^J d \left( \sum_{l=i}^k I_{\{j\}}(b_Y(y_l)), \frac{k-i}{n} \sum_{l=1}^n I_{\{j\}}(b_Y(y_l)) \right) \right]. \quad (23)$$

The edges which give these optimal binnings are given by replacing the max with an arg max. The arguments inside  $d$  are the observed counts of each  $Y$  bin from  $i$  to  $k$  and the expected counts based on the marginal distribution and the relative length of the interval from  $i$  to  $k$ , respectively.

For each  $i \in \{1, \dots, k-1\}$ , this estimate considers two parts. The first part,  $\widehat{D}_{i-1}^*$ , is the previously computed maximal measure on the first  $i-1$  points, with the convention  $\widehat{D}_0^* = 0$ . The second part is a sum of  $d$  over all  $J$  bins of  $\mathbf{b}_{\mathbf{y}}$  with observed counts given by the incidence of each of the  $J$  bins in observations  $i$  to  $k$  and the expected counts given by the marginal distribution of  $\mathbf{b}_{\mathbf{y}}$  multiplied by the length of the interval from  $i$  to  $k$ .

Therefore, this algorithm chooses to add a bin edge at the  $i$  which maximizes Equation (21) conditional on previous bin edges. Additionally, this estimate requires a *pre-specified*  $\mathbf{b}_{\mathbf{y}}$ , and so it does not give a global optimum over all grids. Indeed, it still requires some ad hoc choice of binning on  $\mathbf{y}$ . Jiang et al. (2015) suggests using the slicing methods of Jiang and Liu (2013) to bin  $\mathbf{y}$  while Reshef et al. (2011) suggests a simple equipartition on  $\mathbf{y}$ . The former chooses bins to optimize the difference between the conditional and unconditional variances while the latter is computationally easy to implement.

The main difference between the implementations in Jiang et al. (2015), Heller et al. (2016), and Reshef et al. (2011) is the choice of  $d$ . Jiang et al. (2015) takes a penalized measure

$$d(o_{ij}, e_{ij}) = \frac{o_{ij}}{n} \log \left( \frac{o_{ij}}{e_{ij}} \right) - \frac{\lambda_0}{J} \log n \quad (24)$$

where  $\lambda_0$  is a penalty parameter and the given  $\mathbf{b}_{\mathbf{y}}$  is a binning on  $J$  bins. This is equivalent to a particular prior being placed on the bin locations so that the number of bins follows

a Poisson distribution. [Heller et al. \(2016\)](#) instead take

$$d(o_{ij}, e_{ij}) = \frac{o_{ij}}{n} \log \left( \frac{o_{ij}}{e_{ij}} \right) + \frac{\lambda_0}{J} \log \left( \frac{n-1}{k-1} \right), \quad (25)$$

where  $k$  matches the index  $\widehat{D}_k^*$ . This modification is equivalent to a uniform distribution over all possible marginal binnings. Under both versions of the penalized  $d$ , splits are then considered at each  $x_k$  in turn and the bins which maximize the penalized score are used. In contrast, [Reshef et al. \(2011\)](#) take the unpenalized

$$d(o_{ij}, e_{ij}) = \frac{o_{ij}}{n} \log \left( \frac{o_{ij}}{e_{ij}} \right)$$

and choose to restrict the search space to avoid creating bins which are too small.

Attempts to expand these procedures to optimize over both margins have also been made. [Chen et al. \(2016\)](#) suggest a modified version of the MIC which is guided by the significance of a  $\chi^2$  test to choose the optimal bins. [Cao et al. \(2021\)](#) suggests a backwards merging algorithm on  $\mathbf{b}_y$  to relax the perfect equipartition of [Reshef et al. \(2011\)](#). In both cases, however, an equipartition is the starting point, and so will inevitably impact the final binning.

Given that a conditional and recursive optimization procedure is already the norm, it seems natural to use recursive binary splits to generate a binning as in classification and regression trees and the tree-based binning of [Rahman \(2018\)](#). Recursive binning has several advantages over marginal binning. For one, recursive binning in these contexts can be set to optimize the bin edge choice over both dimensions simultaneously rather than each alone. It also produces more flexible bin arrangements than marginal methods, which can only produce bins aligned along both axes. Finally, recursive splits are adaptive to patterns in the data which are hidden in projections on either axis, suggesting that the method may detect patterns marginal bins miss.

The main problem recursive binning creates is the estimation of expected counts in a bin, which can no longer proceed by taking the product of marginal distributions. However, by first taking the ranks  $\mathbf{r}(\mathbf{x})$  and  $\mathbf{r}(\mathbf{y})$ , the expected count can be determined by the area of the bin directly rather than a marginal product.

## 5 Recursive rank binning to measure association

Consider a pair of variables  $X$  and  $Y$  realized in a sample of  $n$  paired observations  $\mathbf{x}$  and  $\mathbf{y}$ , as in Section 2. Define the vectors of marginal ranks  $\mathbf{s} = \mathbf{r}(\mathbf{x})$  and  $\mathbf{t} = \mathbf{r}(\mathbf{y})$  with

the convention of random tie-breaking for observations with the same rank to avoid ties. Converting to the ranks is equivalent to taking empirical CDF transforms of  $X$  and  $Y$  so that the joint distribution of  $\mathbf{s}$  and  $\mathbf{t}$  is the empirical copula of  $X$  and  $Y$  with a uniform joint distribution under independence. Specifically, this means the expected number of points in a region of  $\{1, \dots, n\}^2$  is equal to the region's area divided by  $n$  under the null hypothesis of no dependence. This conversion allows much more flexible partitions to be considered than marginal partitioning. Here, recursive binary splits are proposed on  $\mathbf{s}$  and  $\mathbf{t}$  to take advantage of this flexibility.

To sketch the algorithm, first consider the objects it acts upon. From the perspective of this algorithm, a bin is a rectangular subspace of  $\{1, \dots, n\}^2$  which may contain some pairs from the paired vectors  $\mathbf{s}$  and  $\mathbf{t}$ . It is defined by its lower and upper bounds in each dimension, and has implicit features such as its area, its depth, the number of pairs it is expected to contain under independence, and the number of pairs actually observed within its bounds. The depth of a bin can be understood as the number of recursive calls required to produce it from the initial state: a single bin with bounds of 0 and  $n$  in both dimensions that contains every observation.

At each step, the algorithm is presented with a partition of  $\{1, \dots, n\}^2$  into a collection of bins resulting from the preceding splits made by the algorithm. For each bin, the algorithm must choose whether it should be split, and if so how it should be split. Under completely unrestricted splitting, splits could be made through either of the two margins along any horizontal or vertical line within the bin boundaries. Choosing among the infinite possible splits is accomplished by finding the split optimizing a score function reflecting the goal of the binning. Once a split is chosen for every bin to be split, the algorithm proceeds recursively by considering the resulting partition in the same way. Two choices made by the analyst therefore dictate the final bins produced by the algorithm: the *score* used to choose splits and the *stop criteria* which determine whether a split is made at all.

Using the settings of the following section, this algorithm has a runtime proportional to  $n \log n$  if bin count or area limits are used as the stop criteria. At each step, it searches through each point in each bin, meaning all  $n$  points are considered. In the worst case, this will only halve the bin count and area at each step, and so  $\log n$  splits are required. In any other case, not all  $n$  points will be considered at every depth. If small bins are created early in the procedure, the points they contain will be ignored thereafter.



## 5.1 Splitting bins

Many heuristics exist to choose splits, see [Garcia et al. \(2012\)](#) and [Rahman \(2018\)](#) for surveys, but previous bin-based measures of association have focused on the  $\chi^2$  statistic against independence and the mutual information (MI) ([Reshef et al., 2011](#); [Jiang et al., 2015](#); [Chen et al., 2016](#); [Heller et al., 2016](#); [Cao et al., 2021](#)). As they are designed to measure the discrepancy of observed distributions from expected distributions with minimal assumptions, both are natural choices to measure the dependence present in a sample.

However, these previous works choose only marginal splits on both dimensions, and so must be adapted to the recursive binning framework of [Rahman \(2018\)](#) by defining local versions of both, the *chi score* and *mi score*, to select the optimal split within a bin. It will be proven that, for either score, the optimal split occurs at the coordinate of a point within a bin. To distinguish between the scores and the final statistics, *chi* and *mi* will be used exclusively to refer to the scores computed to determine splitting and  $\chi^2$  and MI will be used to refer to the final statistics computed over all bins.

To define these local scores recall Equation (21),

$$D(\mathbf{b}_x, \mathbf{b}_y) = \sum_{i=1}^I \sum_{j=1}^J d(o_{ij}, e_{ij}),$$

which expresses a functional measuring statistical dependence over  $X$  and  $Y$  as the sum of a function evaluated over the expected ( $e_{ij}$ ) and observed ( $o_{ij}$ ) number of points in the partitions created by marginal binnings  $\mathbf{b}_x$  and  $\mathbf{b}_y$ . By adapting Equation (21) for the  $\chi^2$  and MI statistics to the recursive binning framework, the *chi* and *mi* scores are implied by the form of  $d(o_{ij}, e_{ij})$ . As the bins produced by recursive binary splits are not defined by independent marginal binnings  $\mathbf{b}_x$  and  $\mathbf{b}_y$ , they do not have obvious  $i, j$  indices. Instead, assume the total number of bins is  $n_{bin}$  and (arbitrarily) index the bins by  $i \in \{1, \dots, n_{bin}\}$ . The arguments must also be changed to  $\mathbf{s}$  and  $\mathbf{t}$  to reflect the absence of marginal bins. Together, this gives the modified expression

$$D(\mathbf{s}, \mathbf{t}) = \sum_{i=1}^{n_{bin}} d(o_i, e_i), \tag{26}$$

where  $o_i$  is the number of observations within the  $i^{\text{th}}$  bin and  $e_i$  is the number expected assuming independence. Letting the area of the  $i^{\text{th}}$  bin be  $a_i$ , this is given by  $e_i = a_i/n$ . The *chi score* of each bin is then

$$d(o_i, e_i) = \text{chi}(o_i, e_i) = \frac{(o_i - e_i)^2}{e_i} \tag{27}$$

and the mi score is

$$d(o_i, e_i) = \text{mi}(o_i, e_i) = \frac{o_i}{n} \log \frac{o_i}{e_i}. \quad (28)$$

Either of these scores can be maximized in the proposed recursive binning algorithm to determine the split coordinate.

### 5.1.1 Maximizing scores

In more detail, denote the  $o_i$  pairs of ranks in bin  $i$  as  $\{(s_{i1}, t_{i1}), (s_{i2}, t_{i2}), \dots, (s_{io_i}, t_{io_i})\}$  and its  $s$  bounds  $(l_s, u_s]$  and  $t$  bounds  $(l_t, u_t]$ . Bin  $i$  can be split either by a vertical line at  $c_s \in (l_s, u_s)$  or a horizontal line at  $c_t \in (l_t, u_t)$  resulting in two new bins with two new chi or mi scores. Denote the observed and expected values for the bin above  $c_s$  as  $o_{i+}(c_s)$  and  $e_{i+}(c_s)$  respectively (analogously, those above  $c_t$  as  $o_{i+}(c_t)$  and  $e_{i+}(c_t)$ ), and use the subscript  $i-$  in the same way to indicate the new bin below the split. A split at  $c$  changes the total score measured by  $d(\cdot, \cdot)$  for the region  $(l_s, u_s] \times (l_t, u_t]$  by

$$\delta_i(c, d) = d(o_{i+}(c), e_{i+}(c)) + d(o_{i-}(c), e_{i-}(c)) - d(o_i, e_i), \quad (29)$$

and so the maximizing split coordinate along a given dimension is

$$c^* = \arg \max_c \delta_i(c, d) = \arg \max_c \left[ d(o_{i+}(c), e_{i+}(c)) + d(o_{i-}(c), e_{i-}(c)) \right].$$

Though  $e_{i+}(c)$  and  $e_{i-}(c)$  vary continuously in the split coordinate  $c$ , both of  $o_{i+}(c)$  and  $o_{i-}(c)$  change only when  $c$  corresponds with the coordinate of a point contained in bin  $i$ , in other words when  $c_s \in \{s_{i1}, s_{i2}, \dots, s_{io_i}\}$  or  $c_t \in \{t_{i1}, t_{i2}, \dots, t_{io_i}\}$ . This has important consequences to selecting splits for both the mi and chi scores.

**Proposition 1** (The split maximizing the chi score occurs at the coordinate of a point within a bin.). *The split coordinate  $c$  which maximizes  $\delta_i(c, \text{chi})$  is the coordinate of one of the points within the bin.*

*Proof.* Without loss of generality, consider a split at  $c_s \in (s_{ij}, s_{i,j+1})$  between the  $j$  and  $j+1$  horizontal coordinates in bin  $i$ . As the split is made between point coordinates  $j$  and  $j+1$ , the observed number of points above is  $o_{i+} = o_i - j$  and the observed number below

is  $o_{i-} = j$  by definition. Substituting Equation (27) into Equation (29) gives

$$\begin{aligned}\delta_i(c_s, \text{chi}) &= \frac{(o_{i+} - e_{i+}(c_s))^2}{e_{i+}(c_s)} + \frac{(o_{i-} - e_{i-}(c_s))^2}{e_{i-}(c_s)} - \frac{(o_i - e_i)^2}{e_i} \\ &= \frac{o_{i+}^2}{e_{i+}(c_s)} - 2o_{i+} + e_{i+}(c_s) + \frac{o_{i-}^2}{e_{i-}(c_s)} - 2o_{i-} + e_{i-}(c_s) - \frac{o_i^2}{e_i} + 2o_i - e_i, \\ &= \frac{(o_i - j)^2}{e_{i+}(c_s)} + \frac{j^2}{e_{i-}(c_s)} - \frac{o_i^2}{e_i}\end{aligned}$$

as  $e_{i+}(c) + e_{i-}(c) = e_i$  and  $o_{i+} + o_{i-} = o_i$ .

The derivative of  $\delta_i(c_s, \text{chi})$  with respect to  $c_s$  can be determined with the help of a few observations. First,  $e_{i+}(c_s) = (u_s - c_s)(u_t - l_t)/n$  and  $e_{i-}(c_s) = (c_s - l_s)(u_t - l_t)/n$  so that  $\frac{d}{dc}e_{i+}(c_s) = -\frac{d}{dc}e_{i-}(c_s)$ . Furthermore, both of the observed counts and the final term in the sum are constant in  $c_s$  for the restricted range considered, and so all have a derivative of zero. Therefore

$$\frac{d}{dc}\delta_i(c_s, \text{chi}) = -\frac{o_{i+}^2}{e_{i+}^2(c_s)}\frac{d}{dc}e_{i+}(c_s) - \frac{o_{i-}^2}{e_{i-}^2(c_s)}\frac{d}{dc}e_{i-}(c_s) = \left[ \frac{o_{i+}^2}{e_{i+}^2(c_s)} - \frac{o_{i-}^2}{e_{i-}^2(c_s)} \right] \frac{d}{dc}e_{i-}(c_s)$$

which simplifies to

$$\frac{d}{dc}\delta_i(c_s, \text{chi}) = \frac{n}{u_t - l_t} \left[ \frac{o_{i+}^2}{(u_s - c_s)^2} - \frac{o_{i-}^2}{(c_s - l_s)^2} \right]$$

with a second derivative

$$\frac{d^2}{dc^2}\delta_i(c_s, \text{chi}) = \frac{2n}{u_t - l_t} \left[ \frac{o_{i+}^2}{(u_s - c_s)^3} + \frac{o_{i-}^2}{(c_s - l_s)^3} \right].$$

As the split coordinate  $c_s \in (s_{ij}, s_{i,j+1})$  is necessarily restricted to within the bin bounds  $(l_s, u_s]$ , both  $c_s - l_s > 0$  and  $u_s - c_s > 0$  and so  $\frac{d^2}{dc^2}\delta_i(c_s, \text{chi}) > 0$ . This implies that  $\delta_i(c_s, \text{chi})$  is concave up between the horizontal coordinates of the points within a bin so that any optimum within these bounds must be minimum. As these are continuous functions, this means maximum must occur at one of the boundaries of the interval  $(s_{ij}, s_{i,j+1})$ . As the index  $j$  was chosen arbitrarily, this same argument holds for every interval and so the global maximum must occur at one of these boundaries. These boundaries are defined by the locations of the points contained within the bin, so the maximal split must occur at the coordinate of a point within the bin. The same argument holds identically for the vertical coordinates, a fact easily seen by switching the subscripts.  $\square$

**Proposition 2** (The split maximizing the mi score occurs at the coordinate of a point within a bin.). *The split coordinate  $c$  which maximizes  $\delta_i(c, \text{mi})$  is the coordinate of one of the points within the bin.*

*Proof.* Using the same argument as for Proposition 1, this is true as long as the second derivative of  $\delta_i(c_s, \text{mi})$  with respect to  $c_s$  is non-negative between adjacent observation coordinates. Substituting Equation (28) into Equation (29) gives

$$\delta_i(c_s, \text{mi}) = \frac{o_{i+}}{n} \log \frac{o_{i+}}{e_{i+}(c_s)} + \frac{o_{i-}}{n} \log \frac{o_{i-}}{e_{i-}(c_s)} - \frac{o_i}{n} \log \frac{o_i}{e_i}$$

with a first derivative

$$\frac{d}{dc} \delta_i(c_s, \text{mi}) = \frac{o_{i+}}{n(u_s - c_s)} - \frac{o_{i-}}{n(c_s - l_s)}$$

and a second derivative

$$\frac{d^2}{dc^2} \delta_i(c_s, \text{mi}) = \frac{o_{i+}}{n(u_s - c_s)^2} + \frac{o_{i-}}{n(c_s - l_s)^2} \geq 0.$$

Therefore, the value of  $c_s$  which maximizes  $\delta_i(c_s, \text{mi})$  must correspond to the coordinate of a point within the bin.  $\square$

This means that splits only need to be considered at the points in  $\{(s_{i1}, t_{i1}), (s_{i2}, t_{i2}), \dots, (s_{io_i}, t_{io_i})\}$  to maximize the chi and mi scores, rather than considering the continuum of potential splits in  $(l_s, u_s] \times (l_t, u_t]$ .

### 5.1.2 Empty bins

If splitting occurs at the coordinates of observed points within bins, the observation at the split has ambiguous bin membership. Taking the convention that these observations are counted in the bin below the split, which is consistent with the initial bin bounds  $[0, n]$  in both dimensions, it is impossible for this algorithm to create empty bins below the observed points. This is despite the potential utility of empty bins when detecting association, as large regions without any observations in the rank space are a strong indication of departures from independence.<sup>9</sup>

---

<sup>9</sup>The ability to create empty bins directly is an advantage of the recursive binning algorithm over marginal methods, which cannot do so. Empty regions marginally only reflect the marginal distribution of a variable, and converting to the ranks presents margins without any gaps for both variables.

To remedy this and allow empty bins to be created, a potential split coordinate below the smallest observations horizontally and vertically is added, denote these pseudo-observations as  $s_{i(1)} - 1$  and  $t_{i(1)} - 1$ . Finally, take the convention that a point is included in the lower bin when a split occurs at one of its coordinates. Along  $s$  this gives the maximizing split coordinate

$$c_s^* = \arg \max_{c_s \in \{s_{min} - 1, s_{i1}, \dots, s_{io_i}\}} \delta_i(c_s, d)$$

and similarly

$$c_t^* = \arg \max_{c_t \in \{t_{min} - 1, t_{i1}, \dots, t_{io_i}\}} \delta_i(c_t, d).$$

Of these two maximizing splits, that giving the greater  $\delta_i(c, d)$  is chosen to split bin  $i$ .

### 5.1.3 Controlling minimum bin size

Though not strictly necessary, one may want to control the minimum bin size produced by splits. This requires some balance to be struck between selecting the maximal split and keeping bins at a particular size. This is relevant, for example, if the  $\chi^2$  statistic is applied to the final bins. Supposing  $n_{bin}$  bins are created by the algorithm, the rank space  $[0, n]^2$  with a presumed uniform distribution has been partitioned into  $n_{bin}$  mutually exclusive categories constrained only by the restriction that

$$\sum_{i=1}^{n_{bin}} o_i = n.$$

This setting is similar to the circumstance originally considered by Pearson in his proposal of the  $\chi^2$  test, and so it is natural to assume a  $\chi_{n_{bin}-1}^2$  distribution for the  $\chi^2$  statistic applied to this bins.

Care must be taken with bin size in order to apply this result, however. The  $\chi_{n_{bin}-1}^2$  distribution is only asymptotically valid for the  $\chi^2$  statistic applied to this data and the fit is better the larger the expected counts in each bin. Therefore, the  $\chi^2$  distribution is typically only applied to the  $\chi^2$  statistic when the expected number of points in each partition is greater than or equal to five (Cochran, 1952). This motivates a floor on the bin size at an expected value of five.

The preceding maximization logic provides no such guarantees, and so restrictions on the candidate splits must be introduced to control the minimal bin size. Rather than

change the score function, this can be accomplished by changing the  $\delta_i(c, d)$  function used to evaluate splits. Consider the modified function

$$\delta'_i(c, \text{chi}, z) = I_{[z, \infty)^2} \left( (e_{i+}(c), e_{i-}(c))^T \right) \delta_i(c, \text{chi}) \quad (30)$$

that forces the change of score to be zero if either  $e_{i+}(c) < z$  or  $e_{i-}(c) < z$ , where  $I_A(x)$  is the indicator function of  $x \in A$ . This change works because  $\delta_i(c, \text{chi}) \geq 0$ , as

$$\begin{aligned} \frac{(o_i - e_i)^2}{e_i} &= \frac{([o_{i+}(c) - e_{i+}(c)] + [o_{i-}(c) - e_{i-}(c)])^2}{e_i} \\ &\leq \frac{[o_{i+}(c) - e_{i+}(c)]^2}{e_i} + \frac{[o_{i-}(c) - e_{i-}(c)]^2}{e_i} \\ &\leq \frac{[o_{i+}(c) - e_{i+}(c)]^2}{e_{i+}(c)} + \frac{[o_{i-}(c) - e_{i-}(c)]^2}{e_{i-}(c)} \end{aligned}$$

by the triangle inequality and because  $e_{i+}(c) \leq e_i$  and  $e_{i-}(c) \leq e_i$ . Therefore, splits producing bins that are too small will give scores less than or equal to the scores produced by all other splits. Taking  $z = 5$  restricts bin splits to follow standard practice.

Controlling the bin size for  $\delta_i(c, \text{mi})$  requires a different convention, as

$$\begin{aligned} \frac{o_i}{n} \log \frac{o_i}{e_i} &= \frac{o_i}{n} \log \left[ \frac{o_{i+}(c)}{o_i} \frac{o_i}{e_i} + \frac{o_{i-}(c)}{o_i} \frac{o_i}{e_i} \right] \\ &\leq \frac{o_i}{n} \left[ \frac{o_{i+}(c)}{o_i} \log \frac{o_i}{e_i} + \frac{o_{i-}(c)}{o_i} \log \frac{o_i}{e_i} \right] \\ &\leq \frac{o_{i+}(c)}{n} \log \frac{o_{i-}(c)}{e_i} + \frac{o_{i+}(c)}{n} \log \frac{o_{i+}(c)}{e_i} + \frac{o_{i-}(c)}{n} \log \frac{o_{i-}(c)}{e_i} + \frac{o_{i-}(c)}{n} \log \frac{o_{i+}(c)}{e_i} \end{aligned}$$

which may be greater than  $\frac{o_{i+}(c)}{n} \log \frac{o_{i+}(c)}{e_{i+}(c)} + \frac{o_{i-}(c)}{n} \log \frac{o_{i-}(c)}{e_{i-}(c)}$ . However, noting that  $\text{mi}(o_i, e_i)$  and  $\text{chi}(o_i, e_i)$  are both independent of the split line  $c$ , maximization of  $\delta_i(c, \text{chi})$  and  $\delta_i(c, \text{mi})$  depends only on the post-split scores  $\text{mi}(o_{i+}(c), e_{i+}(c)) + \text{mi}(o_{i-}(c), e_{i-}(c)) \geq 0$  and  $\text{chi}(o_{i+}(c), e_{i+}(c)) + \text{chi}(o_{i-}(c), e_{i-}(c)) \geq 0$ . Splitting to control the minimum bin size can therefore proceed with indicators by taking the larger of

$$c_s^* = \arg \max_{c_s \in \{s_{\min} - 1, s_{i1}, \dots, s_{io_i}\}} I_{[z, \infty)^2} \left( (e_{i+}(c_s), e_{i-}(c_s))^T \right) [d(o_{i+}(c_s), e_{i+}(c_s)) + d(o_{i-}(c_s), e_{i-}(c_s))]$$

and

$$c_t^* = \arg \max_{c_t \in \{t_{min}-1, t_{i1}, \dots, t_{io_j}\}} I_{[z, \infty)^2} \left( (e_{i+}(c_t), e_{i-}(c_t))^T \right) [d(o_{i+}(c_t), e_{i+}(c_t)) + d(o_{i+}(c_t), e_{i+}(c_t))]$$

when  $d \in \{\text{chi}, \text{mi}\}$ . In the case where all splits are tied on both margins, the bin is halved on a random margin at

$$\text{ceiling} \left( \frac{l+u}{2} \right)$$

regardless of the distribution of points within the bin.<sup>10</sup>

## 5.2 Stop criteria

At each recursive step, a bin is split only if it fails to meet a set of stop criteria. These can include the bin area, number of points in the bin, and the depth of the bin<sup>11</sup>. If, for example, the criteria are a depth of 5 or  $n_i < 10$ , a bin with a depth of 5 or a bin with 10 or fewer points will not be split. Any bin which does not satisfy the stop criteria is split in two and the splitting algorithm is again called on both of the resulting bins.

If bin size is restricted such that  $e_i \geq z \forall i \in \{1, \dots, n_{bin}\}$ , the corresponding stop criterion to prevent the creation of bins below this minimum size is  $e_i < 2z$ . When  $e_i < 2z$ , any split will produce at least one bin with an expected count smaller than  $z$ . Even if there is no restriction  $e_i \geq z$  when splitting, it is advisable to incorporate one in the stop criteria to limit the creation of very small bins.

In all of the following examples, two stop criteria were held constant. Splitting was always stopped when  $n_i = 0$  or  $e_i \leq 10$ . To explore the performance of the algorithm over successive splits, the depth criterion was varied from 2 to 10. For smaller sample sizes, the maximal 1024 bins implied by the depth limit of 10 was never achieved due to the stop criteria for area and empty bins.

## 6 An iterative version

Though it was conceived recursively, an iterative implementation of the algorithm outlined in Section 5 is detailed here. First, consider the outer wrapper function to oversee arbitrary

---

<sup>10</sup>Choosing a random split is another obvious tie-breaking convention, but can force splits which violate the minimum size restriction.

<sup>11</sup>Where “depth” is the number of recursive binary splits needed to create the bin from the original data.

splitting and stopping, presented in Algorithm 1. This wrapper acts on a list of `bin` objects, each with elements:

- `bounds`: named list of upper and lower bounds on  $s$  and  $t$
- `s`: marginal ranks on  $x$  of observations in the bin
- `t`: marginal ranks on  $y$  of observations in the bin
- `e`: expected number of points in the bin
- `depth`: number of recursive splits required to create the bin.

While any bins in a list fail to satisfy the stop criteria, this wrapper calls the splitting function on those bins and combines the resulting new bins with those already stopped. The new bins are then checked against the stop criteria. To initialize, all observations are placed in a bin with bounds of  $(0, n]$  in both dimensions.

Of course, the splitting and stopping logic described in Sections 5.1 and 5.2 are at the heart of this algorithm. Algorithm 2 presents pseudo-code for the splitting logic. The stopping logic is not given a pseudo-code version, as it only involves computing and checking numerous properties of each bin against a pre-determined set of thresholds. Section 7 discusses a particular implementation of this in the R programming language.<sup>12</sup>

Finally, Algorithm 3 gives the pseudocode for a chi scoring function with limited minimal bin size. As written, this function would be provided as the `score` in the `maxScoreSplit` function of Algorithm 2. Note that this algorithm has been written for the chi score but provides a framework for any scoring function. The specifics of line 14 can be replaced with any objective function, for example the mi score of Equation (28) with  $\frac{o_i}{n-3} \log \frac{o_i}{e_i} + \frac{n-3-o_i}{n-3} \log \frac{n-3-o_i}{e-e_i}$  to maximize the marginal Kullback-Liebler divergence from uniformity.

This framework also supports random binning. Rather than computing a function that compares the observed distribution to a uniform one about a split, the scores can be replaced with independent and identically distributed  $U[0, 1]$  realizations. The coordinate of the maximum score value will then be uniformly distributed along each potential split coordinate and each margin, creating a fully random recursive binning procedure. Additionally, as these random realizations are greater than or equal to zero, adopting the

---

<sup>12</sup>In this implementation, there is the ability to specify a custom initial split function with the argument `init`. Choosing `init` to randomly halve a bin along one margin coincides with the splitting logic described earlier, as every split produces a score of zero for the initial uniform data.



---

**Algorithm 1** Iterative binning wrapper

---

**Input**

- $\mathbf{x}$  - vector of observed values in  $x$
- $\mathbf{y}$  - vector of observed values in  $y$ , paired with  $x$
- stopper** - function which tests a list of bins against the stop criteria
- 5: **splitter** - function which performs a binary split on a bin
- init** - (possibly) different splitting function applied to the initial bin with all observations

```
function BINNER( $\mathbf{x}$ ,  $\mathbf{y}$ , stopper, splitter, init)  
   $n \leftarrow \text{length}(\mathbf{x})$  ▷ Compute preliminaries  
   $\mathbf{s} \leftarrow \text{rank}(\mathbf{x})$   
10:  $\mathbf{t} \leftarrow \text{rank}(\mathbf{y})$   
  iniBin  $\leftarrow \text{makeBin}(\mathbf{s} = \mathbf{s}, \mathbf{t} = \mathbf{t}, \text{bounds} = \text{list}(\mathbf{s} = (0, n), \mathbf{t} = (0, n)), \mathbf{e} = n,$   
  depth = 0) ▷ Construct initial bin  
  binList  $\leftarrow \text{init}(\text{iniBin})$  ▷ Initialize bin list  
  stopStat  $\leftarrow \text{stopper}(\text{binList})$  ▷ Initial stop check  
  while any stopStat are FALSE do ▷ Continue as long as bins can be split  
15:   oldBins  $\leftarrow \text{binList}[\text{stopStat}]$  ▷ Stopped bins  
   oldStop  $\leftarrow \text{stopStat}[\text{stopStat}]$  ▷ All TRUE  
   newBins  $\leftarrow \{\}$  ▷ Variable to store splitting results  
   for bin in binList[!stopStat] do  
     append splitter(bin) to newBins ▷ Add split results  
20:   end for  
   newStop  $\leftarrow \text{stopper}(\text{newBins})$  ▷ Check stop criteria on new bins  
   binList  $\leftarrow \text{append newBins to oldBins}$   
   stopStat  $\leftarrow \text{append newStop to oldStop}$   
  end while  
25:  return binList  
end function
```

---

---

**Algorithm 2** Score maximizing splitter

---

**Input**

**bin** - the bin object to be split with elements **s**, **t**, **bounds**, **e**, and **depth**  
**scorer** - function accepting a vector of coordinates in increasing order and the expected number of points in **bin** and returning a vector of scores corresponding to splits at each internal coordinate

```
function MAXSCORESPLIT(bin, scorer)
5:  get s, t, s.bounds, t.bounds, e, depth from bin
   sort s, t in increasing order to give sSrt, tSrt
   cs  $\leftarrow$  append ( sSrt[1]-1, sSrt )
   ct  $\leftarrow$  append ( tSrt[1]-1, tSrt )            $\triangleright$  Add a split coordinate below all points
   ds  $\leftarrow$  scorer( append ( s.bounds[1], cs, s.bounds[2] ), e )
10:  dt  $\leftarrow$  scorer( append ( t.bounds[1], ct, t.bounds[2] ), e )
   sMax, tMax  $\leftarrow$  the indices of the maxima of ds, dt
   if all ds = ds[sMax] AND all dt = dt[tMax] then
     if ds[sMax] > dt[tMax] then
       split bin on s at ceiling(mean(s.bounds))
15:     else if ds[sMax] < dt[tMax] then
       split bin on t at ceiling(mean(t.bounds))
     else
       split bin randomly on s or t at ceiling(mean(s.bounds)) or
       ceiling(mean(t.bounds))
     end if
20:   else if ds[sMax]  $\geq$  dt[tMax] then            $\triangleright$  Ties go to s
     split bin on s at cs[sMax]
   else
     split bin on t at ct[tMax]
   end if
25:   return upper and lower split of bin
end function
```

---

---

**Algorithm 3** Marginal  $\chi^2$  scores

---

**Input**

$\mathbf{x}$  - a numeric vector of potential split coordinates in increasing order  
 $e$  - a numeric value giving the expected number points in a bin  
 $e_{min}$  - the minimum expected number allowed for a split

```
5: function CHISCORING( $\mathbf{x}$ ,  $e$ ,  $e_{min}$ )  
    $n \leftarrow \text{length}(\mathbf{x})$   
    $cumulative \leftarrow \mathbf{x}[2] - \mathbf{x}[1]$   $\triangleright$  Initialize cumulative length  
    $density \leftarrow e / (\max(\mathbf{x}) - \mathbf{x}[1])$   $\triangleright$  Density under uniformity  
    $scores \leftarrow \{\}$   $\triangleright$  Initialize storage  
10: for  $i = 2$  to  $n - 1$  do  
    $e_i \leftarrow cumulative * density$   $\triangleright$  Expected count below  $i$   
    $o_i \leftarrow i - 2$   $\triangleright$  Observed count ignores bounds, pseudo-point  
   if  $e_i \geq e_{min}$  AND  $e - e_i \geq e_{min}$  then  
     append  $\frac{(o_i - e_i)^2}{e_i} + \frac{(n - 3 - o_i - e + e_i)^2}{e - e_i}$  to  $scores$   $\triangleright$  chi score of candidate split  
15:   else  
     append 0 to  $scores$   
     end if  
      $cumulative \leftarrow cumulative + \mathbf{x}[i + 1] - \mathbf{x}[i]$   $\triangleright$  Update length  
   end for  
20: return  $scores$   
end function
```

---

indicator multiplication of Equation (30) controls the bin size under this form of random splitting.

## 7 The AssocBin package

Algorithms 1, 2, and 3 are implemented in the R package `AssocBin` for the mi score, chi score, and random splitting score. The core functions are:

**makeCriteria:** a function which captures its arguments and appends them into a single logical expression

**stopper:** a function which accepts a list of bins and a logical expression and evaluates the expression within each bin using R's lexical scoping

**binner:** the wrapper function described in Algorithm 1 which accepts integer vectors `x` and `y`; a **stopper** function which accepts a list of bins and returns a logical vector; a **splitter** function which accepts a single bin and returns a pair of bins partitioning the input bin; an **init** function which splits the initial bin containing all points; and (optionally) additional arguments to pass to internal function calls

**chiScores, miScores, randScores:** functions which implement Algorithm 3 with line 14 replaced by the corresponding score

**maxScoreSplit:** the splitting function described in Algorithm 2 which accepts a **bin** and **scorer** function in addition to **ties** and **pickMax** which allow for custom specification of how to handle score ties and choose a maximum

**splitX, splitY:** functions which accept a **bin** to be split, a numeric **bd** giving the coordinate of the split, and the indices of values **above** and **below** **bd** and return two bins resulting from a split of **bin** at **bd** along the corresponding margin

**halfCutTie:** the tie-breaking logic described in Algorithm 2

By writing **binner** with fully modular components, the score function, splitting logic, stop criteria, and ties can be modified to suit the preference of a user. As these are all imagined as single argument functions within **binner**, this requires that certain functions be defined in closures before use. To use **stopper**, for example, the stop criteria returned by **makeCriteria** must be passed as an argument to **stopper** within another function

which returns a single-argument function. Similarly, `maxScoreSplit` must have its scoring function and minimum expected count set in a closure that then accepts a single argument. Though this requires some extra set up, it limits the arguments of `binner` and forces the user to consider these choices intentionally in advance. The demos included in the package provide numerous examples of this set up.

Additional helpers visualize and summarize the results. The `binChi` function computes the  $\chi^2$  statistic over a list of bins returned by `binner` and the `plotBinning` function plots a bin list and scatterplot with optional fill. Two additional functions, `depthFill` and `residualFill`, create gradient fills to communicate depth or residual magnitude based on colour range and residual function arguments. Such visualizations not only give insight into what region of the data the algorithm deems most important, but are also useful as a summarized display of the data. Rather than a scatterplot with potentially thousands of points, these visualization display a handful of coloured regions which can be read at a glance. The full package can be found on [the author's GitHub](#).

## 8 Using the algorithm

Some results gained from the implementation of this method in R are presented here. First, a series of visualizations of the algorithm on independent data and strongly associated data are given to demonstrate how it works step-by-step. Then, as both [Heller et al. \(2016\)](#) and [Reshef et al. \(2011\)](#) utilize simulated independent  $X$  and  $Y$  to generate the  $p$ -values of their methods, the null distribution of the recursive binning measure under different splitting rules is explored. This is followed by the application of the method to simulated data patterns from [Newton \(2009\)](#) and [Liu et al. \(2018\)](#). Finally, a real data set is examined.

### 8.1 Simple examples

To illustrate the behaviour of the maximum splitting algorithm from Section 6, consider applying it to two extremes: random independent data and data in perfect agreement. Scatterplots of both of these simulated data sets with  $n = 1,000$  are shown in Figure 2.

As the ranks of both data sets have no gaps, the initial step of the algorithm will not find a marginal maximal split. Indeed, for any split at a point the number of points on either side will match expectation exactly. Therefore, the algorithm begins by splitting the initial bin in half by adding a vertical edge at 500 in both. This gives the bins seen in Figure 3.

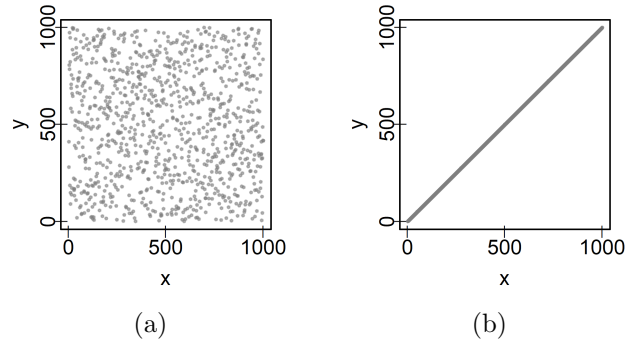


Figure 2: The (a) simulated random data and (b) perfect rank agreement data used to illustrate the flow of the algorithm.

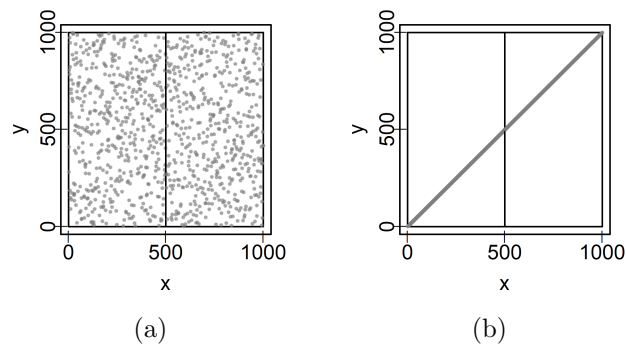


Figure 3: The (a) simulated random data and (b) perfect rank agreement data with the first split indicated.

Once so halved, the ranks are no longer necessarily uniform within the bins. Marginal gaps are introduced in both due to the split. Therefore, the next split is not made at the halfway point, but is instead made to optimize the deviation of counts from uniformity as measured by the score function. While identifying the location of these splits on either side in the random uniform data is difficult, the expected split in the line data would be another halving of the bins, as this produces empty corner bins which should each contain a quarter of the observations. Indeed, this is the result seen in Figure 4.

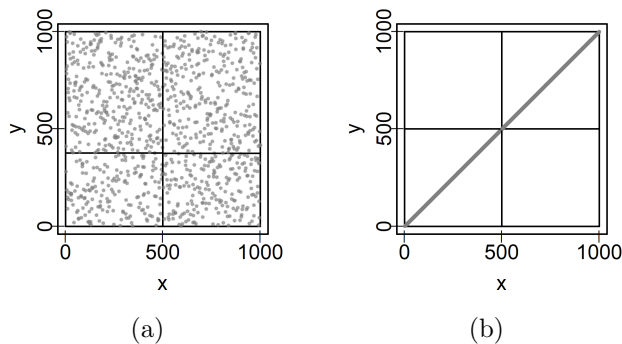


Figure 4: The (a) simulated random data and (b) perfect rank agreement data with the first two splits indicated, dividing both data sets into four bins.

Such a step-by-step demonstration could be continued, to the tedium of the reader, but an easier visualization can summarize such stepwise inspection. For each bin, the implementation described in Section 7 keeps track of the bin depth as well as its other features. More information about the algorithm’s path can be gleaned by simply running the algorithm and shading the bins according to their depth. Setting a maximum depth of six and shading in this way produces Figure 5.

There are stark differences between the depth patterns for these two data sets, as might be expected. While the uniform random data continues splitting every bin somewhat haphazardly with the exception of small early splits that meet the stop criteria (the expected number of observations being 10 or fewer or no observations within the bin), the line data causes a very particular pattern of depths to emerge. It seems to chase the linear pattern by introducing many more splits along its length, in a sense introducing a greater density of bins to the regions with greater density of points.

By chasing these regions, the algorithm produces a striking pattern in the residuals of its final bins. This pattern occurs in, for example, the Pearson residuals of bins with

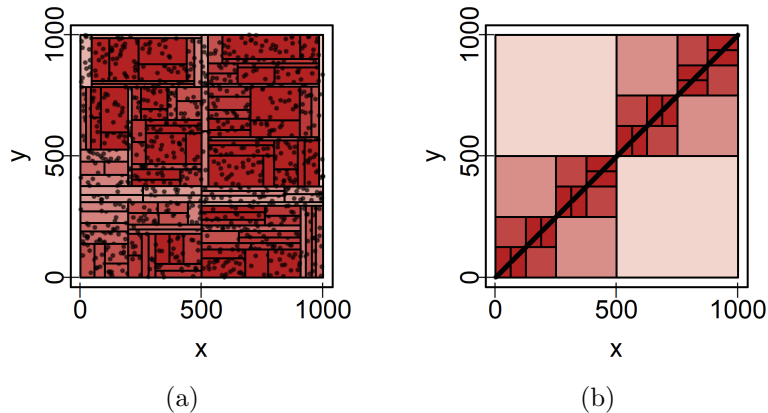


Figure 5: The (a) simulated random data and (b) perfect rank agreement data split to a maximum depth of six, with bins shaded darker according to their depth. The algorithm splits to the maximum depth along the line and not elsewhere while the in the random data continues splitting in every location.

expected counts  $e_i$  and observed counts  $o_i$ ,

$$r_i \text{sign}(o_i - e_i) \sqrt{\frac{(o_i - e_i)^2}{e_i}}.$$

Large positive residuals occur all along the line and large negative ones occur away from it. Figure 6 plots these residuals using hue to convey their sign, with the convention that blue represents negative values and red represents positive ones, and saturation to convey their magnitude, with darker saturation indicating a larger magnitude.

While bins in the random data do not display pronounced shading, indicating small residuals, the line pattern has large positive residuals all along its length and large negative residuals elsewhere. In particular, note the deep blue shading in upper left and bottom right quadrants. Even without the points, the structure of the data is easily discerned from the shading of these bins alone.

In this example, taking a sum of the squared Pearson residuals to get the  $\chi^2$  statistic gives values of 87.8 for the random data and 7000 for the line data. Of course, as the bins produced here do not follow a regular grid pattern and are generated by maximizing a score analogous to the  $\chi^2$ , the distribution of the statistic warrants an investigation under independence. As these bins are produced using optimization at each step, it is not clear



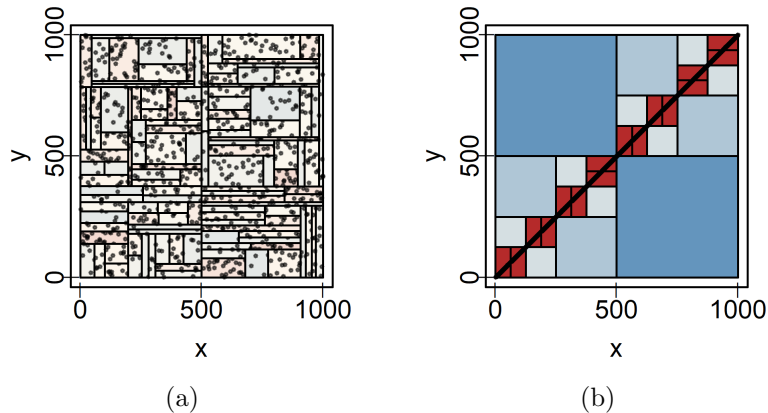


Figure 6: (a) Simulated random data and (b) simulated data with perfect rank agreement split to a maximum depth of six, with bins shaded according to their Pearson residuals. Negative residuals are shaded blue while positive residuals are shaded red, with darker shading indicating a larger residual magnitude. Large positive residuals occur along the line and large negative ones occur elsewhere.

that  $n_{bin}$  bins would have a  $\chi^2$  distribution with  $n_{bin} - 1$  degrees of freedom as is usually the case, even with the controlled minimum bin size.

## 8.2 The null distribution

Even presuming the  $\chi^2$  distribution applied to the  $\chi^2$  statistic on these bins, the degrees of freedom would be given by  $n_{bin} - 1$ . As  $n_{bin}$  is a result of the stop criteria and splitting logic, the null distribution will depend on both of these. The nature of its dependence on the splitting logic is explored here. Three different splitting rules are considered: random splits, chi score maximizing splits, and mi score maximizing splits. All will lead to different final bins when applied to the same data, and therefore different statistic values. To give the  $\chi^2_{n_{bin}}$  distribution a better chance of fitting, all were restricted so that bins with expected counts less than 5 were not created.

Consequently, the null distribution is investigated by generating 10,000 independent bivariate data sets  $\mathbf{x}, \mathbf{y} \in \mathbb{R}^{10,000}$  by randomly and independently shuffling the vector of ranks  $\{1, 2, \dots, 10000\}$  on each margin. Every  $\mathbf{x}, \mathbf{y}$  pair is recursively binned to every maximum depth between two and ten using random binning, binning maximizing the

chi score, and binning maximizing the mi score at each step. Splitting is stopped when the expected number of observations within a bin falls below ten or if a bin contains no observations. For each binning, the  $\chi^2$  statistic is computed for the final bins based on the observed and expected counts, and this statistic is recorded along with the number of final bins.

### 8.2.1 The impact of depth

To start, consider a plot of the  $\chi^2$  statistic against the number of bins for these simulated data when bin splits are selected randomly and uniformly among observed point coordinates within a parent bin. Figure 7 displays this plot with both margins  $\log_{10}$  transformed to make the horizontal width of clusters for small depths as wide as those for large depths. A dashed line is plotted on top of the points at the 99% critical value of  $\chi^2_{n_{bin}-1}$  for reference.

Due to interference by the expected and minimum count stop criteria, the maximum depth stop criterion does not produce the same number of bins every time. If every bin were split at every step, a maximum depth of  $d$  would always produce  $2^d$  bins but small bins are produced by chance which are not further split even when the maximum depth is increased. Nonetheless, a larger maximum depth will produce more bins as long as some can be split. This produces the clusters of bin counts at each depth in Figure 7.

A more interesting result comes from a comparison between the 99% critical value of the  $\chi^2_{n_{bin}-1}$  distribution and statistic values for all depths. Given that 10,000 null cases are generated for each depth, roughly 100 points are expected above this critical value if the 0.99 quantile of the  $\chi^2_{n_{bin}-1}$  corresponds with the 0.99 quantile of the null distribution. Instead, far fewer points are observed above the line. This suggests the  $\chi^2_{n_{bin}-1}$  99% critical value provides a conservative approximation of this critical value for the null distribution under random splitting. That is, choosing quantiles from this distribution to test for dependence at level 0.01 implies a test with a level of at most 0.01 for the null distribution. Indeed, quantile regression performed later suggests the  $\chi^2_{n_{bin}}$  distribution is generally a conservative approximation for the null distribution of the  $\chi^2$  statistic under random splitting.

The same result is not expected for splits chosen to maximize the chi or mi score due to this deliberate maximization. The  $\chi^2$  statistic for the simulated data split to optimize the chi score is shown plotted against the final number of bins in Figures 8 and the same plot for splits optimizing the mi score are shown in 9. Points are, again, coloured according to the maximal depth allowed, and the mean statistic values and number of bins for each of these depth settings are denoted with corresponding coloured squares. Additionally, the

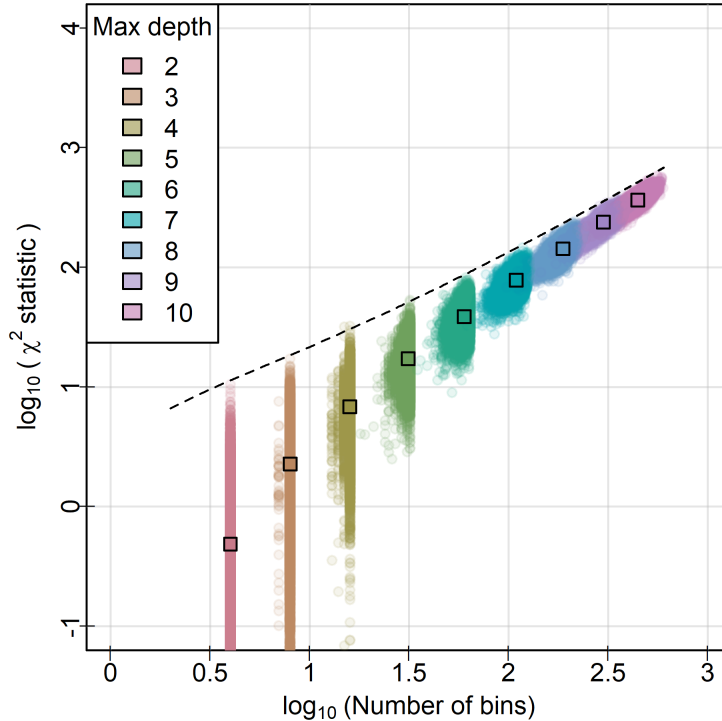


Figure 7: The  $\chi^2$  statistic plotted by the final number of bins for 10,000 simulated independent data sets for each of 9 depth settings with random binnings. The dashed line displays the 99% critical value of the  $\chi^2$  distribution with one degree of freedom less than the number of bins, which is conservative for all depths.

99% critical value for the  $\chi^2$  distribution with  $n_{bin} - 1$  degrees of freedom is plotted against  $n_{bin}$ .

Two changes occur in Figure 8 compared to random binning. First, the statistic values tend to be larger than the null case for the same value of  $n_{bin}$ . Indeed, the majority of score-maximizing binned statistics are above the  $\chi^2_{n_{bin}-1}$  99% critical line when the maximal depth is only 4, all observations are above the line when the depth is 6, and the gap between the critical value curve and the true distribution grows larger as the number of bins increases.

Second, the number of bins no longer displays clear separation by the restriction on maximal depth. Whereas Figure 7 has clusters along the horizontal margin corresponding

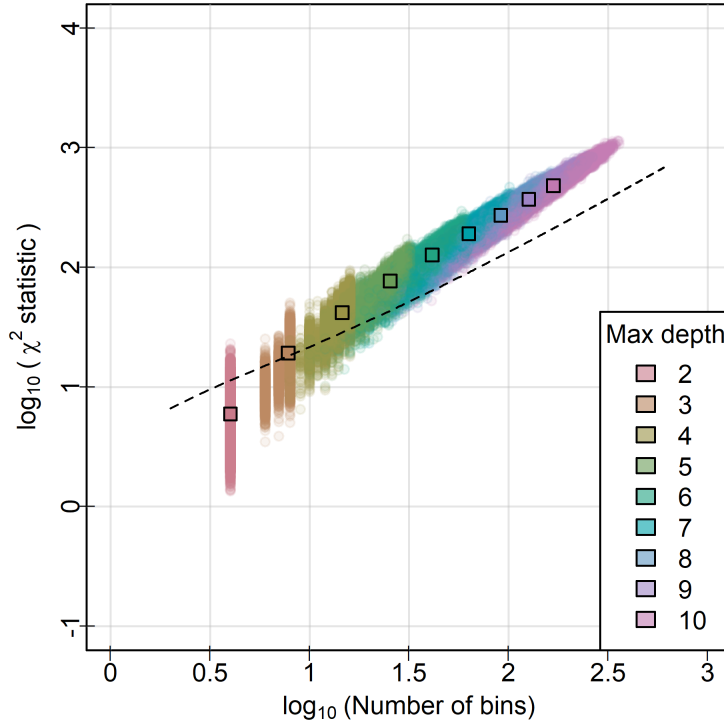


Figure 8: A comparison of the number of final bins and  $\chi^2$  statistic for 10,000 simulated independent data sets split to maximize the chi score over each of 9 depth settings. The dashed line displays the 99% critical value of the  $\chi^2$  distribution with one degree of freedom less than the number of bins. For all depths, many more points lie above this critical value than would be expected if the data followed a  $\chi^2_{n_{bin}-1}$  distribution.

to each maximal depth, the maximum binning bin counts are not strongly grouped. This may be a result of the maximized method selecting smaller bins on average than random binning, resulting in fewer bins due to the minimum size and expected count restrictions that stop splitting of these small bins early. This dynamic ‘smears’ the number of bins for each maximum depth, leading to large overlap between groups by maximum depth.

Figure 9 shows a similar pattern for the mutual information statistic. The  $\chi^2$  statistic value rapidly increases in the number of bins, resulting in a distribution which is well above the  $\chi^2_{n_{bin}-1}$  0.99 quantile. Indeed, both seem to produce similar null distributions for the  $\chi^2$  statistic when applied to the same data.

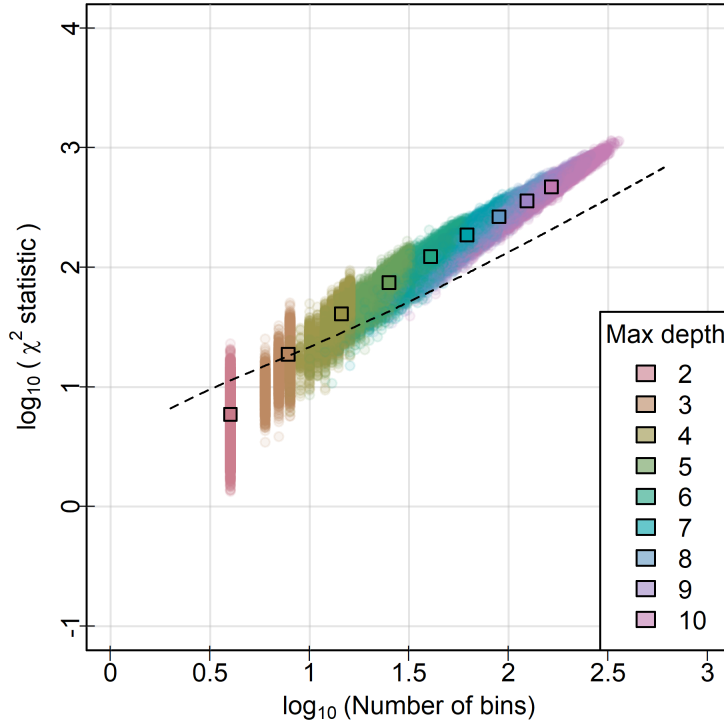


Figure 9: A plot of the  $\chi^2$  statistic by the final number of bins for a binning which maximized the mi score at each step. The plot looks almost identical to that generated by splitting the chi score.

To better compare the  $\chi_{n_{bin}-1}^2$  quantiles to the null distributions across all numbers of bins, quantile regression of the statistic value on the bin depth was carried out using simulated data and the `quantreg` package in R (Koenker, 2023). Specifically, regression of the 0.95, 0.99, and 0.999 quantiles of the  $\chi^2$  statistic was carried out for binning under all three splitting methods. The results are shown in Figure 10. Just as indicated by the earlier plots, maximized splitting with either score leads to *inflated* statistic values, that is statistic which is stochastically greater than a  $\chi_{n_{bin}-1}^2$  random variable. Both maximized methods produce almost identical upper quantiles. In contrast, random splitting produces a  $\chi^2$  statistic which is stochastically less than a  $\chi_{n_{bin}-1}^2$  random variable, suggesting the  $\chi_{n_{bin}}^2$  distribution could be used to generate conservative  $p$ -values (at least in the tails).

These lines not only make the difference in the distributions under the different splitting

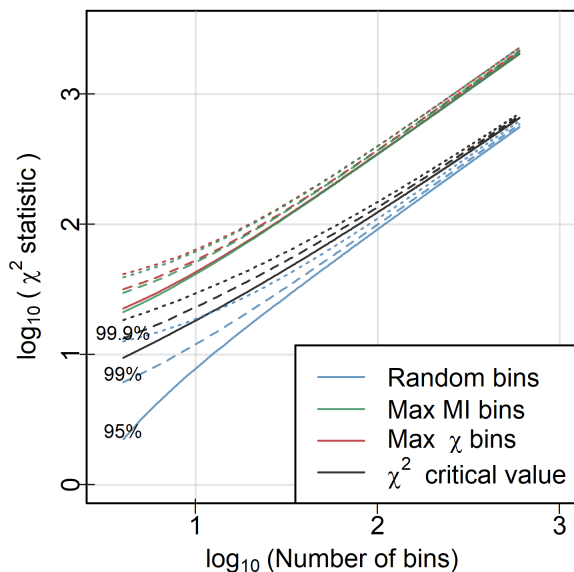


Figure 10: Fit quantile regression lines for several quantiles for all different splitting methods. Both maximized splitting methods lead to similar larger quantiles that grow faster with depth and are further apart, though the chi score leads to slightly larger  $\chi^2$  statistic values.

methods clear, but also could be used in practice to determine rejection or acceptance of the null hypothesis of independent data. Of course, the quantiles depend on the number of observations, so this plot is only demonstrative unless the sample size is 10,000.

In short, both depth and splitting method are highly relevant to the distribution of statistics computed on the final bins. The naive  $\chi^2_{n_{bin}-1}$  distribution on the bins seems to provide a conservative distributional approximation for random splitting, if any maximization is used it cannot be used for accurate rejection or to approximate  $p$ -values. Indeed, the critical value of the statistic in this case generated must take the number of bins into account. Most simply, a large simulation as performed here can be used as a reference and the empirical distributions could be used to generate critical values or empirical  $p$ -values for each number of bins. These could be smoothed or interpolated to cover gaps in the data due to certain bin counts occurring less frequently by chance.

### 8.3 Depth and sample size

To investigate other sample sizes, 10,000 samples of both size  $n = 100$  and  $n = 1,000$  were generated and split to a maximum depth of 10. Random binning and binning maximizing the chi score were applied to the collection of samples for both sample sizes with the same stop criteria as the null investigation immediately preceding. Plots of the resulting  $\chi^2$  statistic and number of bins are compared to the plot for  $n = 10,000$  in Figure 11 for the case of random splitting and in Figure 12 for the case of spitting which maximizes the chi score at each step. Splits maximizing the mi score were not investigated here due to the very similar null distribution between the null under these splits and when maximizing the chi score.

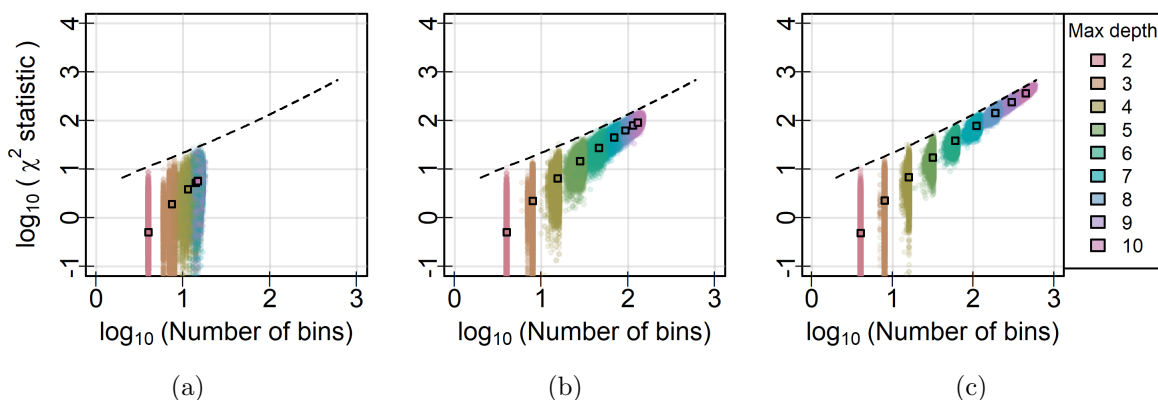


Figure 11:  $\chi^2$  statistic and number of bins for 10,000 samples of simulated random data split by random binning to a maximum depth of ten with the minimum expected bin count restricted to 5 for (a)  $n = 100$ , (b)  $n = 1,000$ , and (c)  $n = 10,000$ . As the sample size increases, the maximum number of bins and separation between the depths increases.

In both cases, the primary impact of increasing the sample size is to increase the maximum number of bins produced by the algorithm. For smaller sample sizes, the minimum bin size stop criteria and bin split restrictions end splitting before many bins are created. This could have been anticipated. With a sample size of 100, for example, splitting the data into 10 bins implies an expected count of 10 per bin, at which point the stop criteria would cease further splitting. Irregular bin shapes complicate this, of course, but the basic idea stands. Fewer points means smaller expectations to compare to the constant stop criteria.

Importantly, this does not seem to impact the conservative approximation of the  $\chi^2$

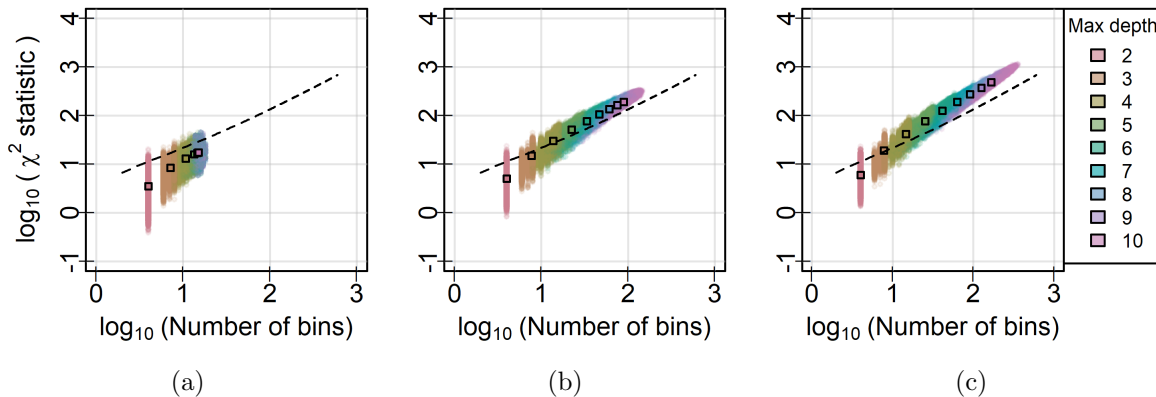


Figure 12:  $\chi^2$  statistic and number of bins for 10,000 samples of random data split maximizing the chi score with a minimum expected bin count of 5 to a maximum depth of ten for (a)  $n = 100$ , (b)  $n = 1,000$ , and (c)  $n = 10,000$ . As before, the sample size limits the maximum number of bins produced by the algorithm.

statistic under random binning by the  $\chi^2_{n_{bin}-1}$  distribution. For all three sample sizes, the observed statistic values have similar location and spread given the number of bins. As the sample size increases, the statistics merely spread along the curve dictated by the  $\chi^2_{n_{bin}-1}$  distribution.

A more impactful pattern is seen for splitting maximizing the  $\chi^2$  score. As the sample size increases, the whole distribution of the  $\chi^2$  statistic moves upward for a given number of bins. This is particularly obvious if the mean points are compared to the line providing the 99% quantile of the  $\chi^2_{n_{bin}-1}$  distribution. In Figure 12(a), none of the mean points lie above this line for  $n_{bin} > 10$  while in Figure 12(c) all of them lie well above this line.

These different behaviours are probably a result of the way the chi score maximizing algorithm chases local patterns, as demonstrated on the perfect line data. Random binning splits agnostically, but chi maximizing binning searches through all splits for the one leading to the largest  $\chi^2$  statistic. Large  $\chi^2$  values therefore occur by chance for random binning but are actively sought by maximized binning. With a larger sample, a greater variety of local patterns will be included in any realization which can inflate the  $\chi^2$  statistic. The maximized algorithm actively searches for such patterns, stochastically increasing the resulting distribution.



## 8.4 Simulated data patterns

Besides the null distribution, an important aspect to the use of recursive binning to measure association is the ability of the algorithm to detect non-null patterns in the data. [Newton \(2009\)](#) provides supplemental code to generate several interesting data patterns, which have since been used by [Liu et al. \(2018\)](#) and [Heller et al. \(2016\)](#) to test their methods and also appear on the Wikipedia article for [Pearson's correlation](#). This code is adapted and used here to repeatedly generate observations following each pattern as a test of recursive binning. Samples of 1,000 observations from each pattern are shown in [Figure 13](#), and the marginal ranks of these samples are shown in [Figure 14](#). Both figures have the margins dropped for brevity.



Figure 13: Point patterns used in [Newton \(2009\)](#) and [Liu et al. \(2018\)](#) to demonstrate different dependence structures. In the last pattern, the data are independent despite the obvious two-dimensional structure.



Figure 14: The patterns of [Figure 13](#) converted to marginal ranks. Refer to these patterns as the wave, rotated square, circle, valley, cross, ring, and uniform noise respectively.

All but the final pattern contain non-linear dependence between the vertical and horizontal variables, and still display strong patterns when these variables are converted to ranks. The final sample, in contrast, consists of four clusters of equal size which can be constructed by the product of independent bimodal marginal densities. Consequently, in the ranks the sample appears uniform. The final pattern therefore acts as a control to

ensure that structure without dependence is not detected by recursive binning applied to the ranks.

For each pattern, both the chi score maximizing binning and random binning algorithms were applied with maximum depths ranging from 1 to 10 and the same stop criteria as previously (stop splitting for bins with an expected count of ten or less and empty bins). This gives a sequence of  $n_{bin}$ ,  $\chi^2$  coordinates for each pattern as the depth restriction is increased, just as in Figures 7 and 8. Rather than visualize these as points, the progression of bins and statistics with increasing maximum depth can be emphasized by joining the points for successive depth restrictions to give paths for each pattern in the  $n_{bin}$ ,  $\chi^2$  space. The same can be done for the 10,000 simulated null samples of 1,000 points from Section 8.2 to give 10,000 null lines for comparison. Figure 15 displays paths coloured by pattern to match Figure 14 alongside the null paths coloured in gray. A dashed line at the 0.95 quantile of the  $\chi^2_{n_{bin}}$  distribution is added to simulate a rejection boundary in Figure 15(b).

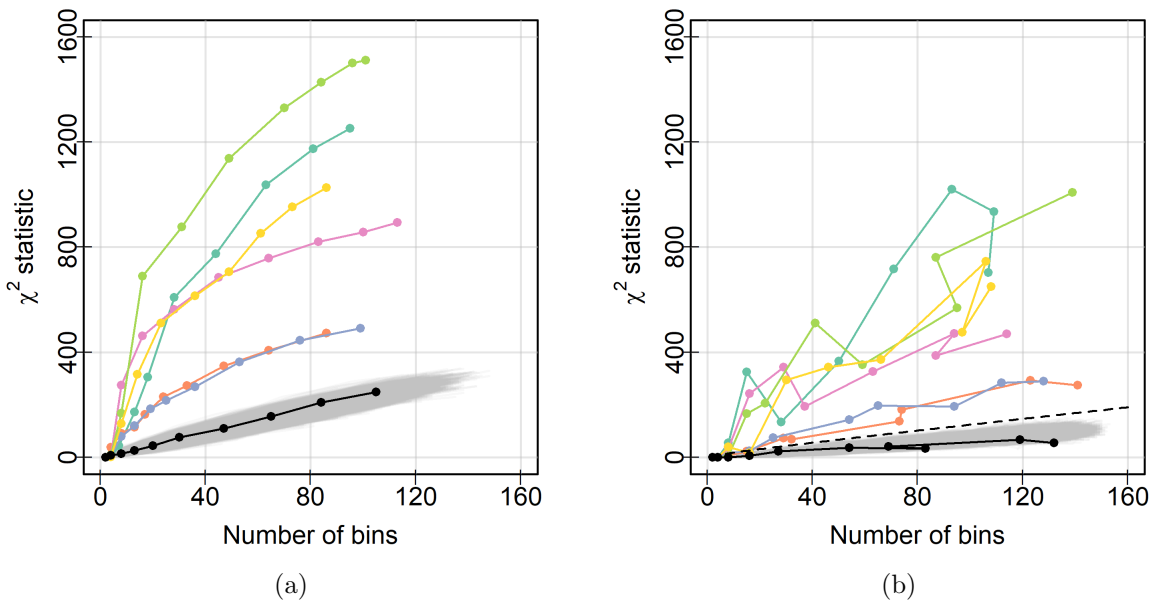


Figure 15: Paths for every pattern in  $n_{bin}$ ,  $\chi^2$  statistic space across depth restrictions for (a) maximized chi score splitting and (b) random splitting. While the maximized splitting is deterministic for a sample, leading to smooth curves, randomized binning leads to rough and erratic paths. Despite this, both display roughly the same ordering of the patterns by colour, and all patterns have paths far above any of the 10,000 simulated null cases.

Figure 15(a) shows smooth curves increasing in both the number of bins and the  $\chi^2$  statistic as the maximum depth is increased while Figure 15(b) shows erratic paths which occasionally decrease in the statistic value as depth increases. Holding this major difference aside for a moment, all the curves for patterns with dependence lie well above the null paths, while the uniform pattern sits within the null curves for both splitting methods. This suggests empirical  $p$ -values less than 0.0001 for every pattern when the depth restriction is greater than 3. Additionally, the order of the curves is similar between the two, with the wave and the cross giving the largest  $\chi^2$  statistic values for a given number of bins and the rotated square and circle giving the smallest statistic values.

Returning to the difference in path smoothness, the erratic nature of the random binning and smoothness of the maximized binning are natural consequences of the different split methods. The maximized splitting algorithm chooses the maximum split at each step and so behaves deterministically for a given sample. In contrast, the random splitting algorithm proceeds non-deterministically and will generate different bin counts and statistic values for a given depth restriction every time it is run, even for constant data. To better see the difference this makes for the separation of the patterns and to evaluate the performance of both based on more than a single exemplar, samples of 1,000 points from each pattern are generated independently and subsequently split either by chi-maximizing or random binning. The resulting paths for each of the 100 independent samples are displayed in Figure 16, with the median path plotted using a thicker grey-accented line.

The clouds of paths show roughly the same ordering under both random binning and chi-maximized binning. Both place the wave (in dark green) and the cross (in light green) above the others, followed closely by the valley (in pink) and the ring (in yellow). Halfway between these these patterns (all with locally linear sections) and the null patterns sit the rotated square (in orange) and circle (in blue). Though these latter two result in smaller statistic values than the others, they remain easily distinguished from the null paths in both Figures 16(a) and 16(b). Indeed, under random splitting the  $\chi^2_{n_{bin}-1}$  0.95 quantile plotted with a dashed line neatly separates the null paths from these two patterns and consequently all patterns.

The close agreement of their ordering suggests that randomized binning is as powerful as maximized binning at detecting these patterns. The clear separation of the null curves from the curves of all patterns over all repetitions implies empirical  $p$ -values  $< 0.0001$  for all patterns when the algorithm is allowed to reach its maximal depth using only bin size stop criteria. Any of these patterns would therefore be regarded as significant by both regimes for commonly used rejection levels. Moreover, as the order of curves by pattern is the same for both, the greatest difference between the maximized binning and random binning seems to be the increased the statistic value alone. If a rejection level is chosen

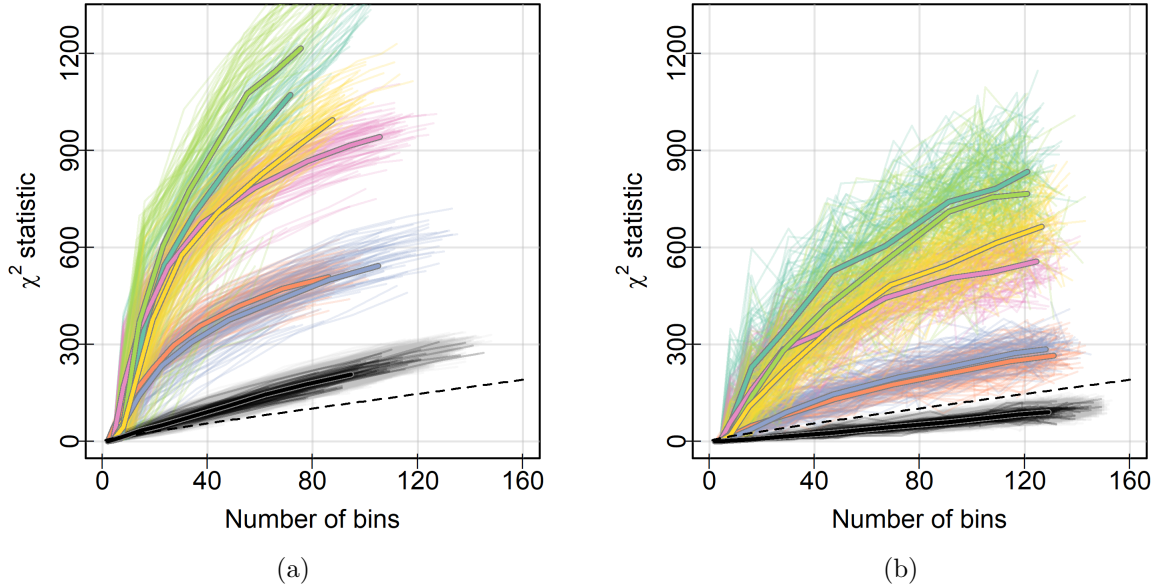


Figure 16: Paths of (a) maximized and (b) random binning applied to 100 independent realizations of the seven simulated data patterns compared to the null paths with median paths plotted with thicker lines accented by grey. Both splitting regimes create clear separation between the null paths and paths of patterns with dependence and both display the same ordering of patterns. The random splitting, however, creates more erratic and variable paths.

on the  $\chi^2$  statistic proportional to the null quantile, we expect that both regimes would show the same tendency for acceptance or rejection of every pattern. Given that random binning requires less computation and has a conservative  $p$ -value provided by the  $\chi_{n_{bin}-1}^2$  distribution, the similar ordering of these curves provides a strong argument for the use of random recursive binning of the ranks to detect and quantify dependence between variables.

#### 8.4.1 Progression of bins in the maximizing algorithm

The median lines are somewhat more interesting, as they cross each other frequently. This suggests the ordering of these different patterns, and potentially the power of the algorithm under each splitting method to detect them, is dependent on the maximum depth. Under chi-maximized binning, the median line for the rotated square is above all others for very

small numbers of bins, indicating there is a pattern in the data which can be captured quickly with few splits. In contrast, the median line for the ring pattern starts below most others for both splitting methods, indicating that a certain number of bins are required before the pattern is detected. It seems each pattern has a natural *resolution*: a number of bins required to identify the dependence.

Directly related are the different slopes of these curves for each pattern. Patterns which generate large residuals within a few splits will grow rapidly at first, and then may slow if the following residuals are relatively small. The median path of the valley pattern, for example, grows quicker than most other patterns in the number of bins for the first few depths before its rate of growth slows. In contrast, the  $\chi^2$  statistic of the ring pattern is unexceptional before a certain depth, at which point the statistic values jump abruptly. More insight into both the slope of these lines and the resolution of each pattern can be gleaned by plotting the bins at each depth for each pattern shaded by residual as in Figure 17.

As before, the hue of the shading is determined by the sign of the bin’s Pearson residual, blue for negative and red for positive, and the saturation is determined by its magnitude. To ensure fair comparison of the residuals, all saturations are determined relative to the maximum residual observed across all depths. The rapid early growth of the rotated square can be spied immediately by its shading in the first row. After only two splits, the empty top left corner and dense top right are detected by the maximized binning algorithm and contribute large residuals, leading to a large early  $\chi^2$  statistic. Once these regions of low and high density around the margins are identified everywhere, however, the algorithm is left splitting the nearly uniform interior of the rotated square, and so grows parallel to the null paths. One interpretation of this “elbow” point is the point at which the recursive binning has adequately captured the pattern in the data. Additional splits beyond this point are ineffective at increasing the score because they occur essentially randomly based on previous splits.<sup>13</sup>

In contrast, the pattern observed for the ring requires a certain depth to detect. The radial symmetry of this pattern means that most early splits fail to identify the less dense regions in the corners and the centre and the more dense region along the circumference of the ring. It is only as the depth exceeds 6 that strong positive and negative residuals are found in any bins, before that point the residuals are not as large as for the other patterns.

---

<sup>13</sup>Another interpretation of this behaviour is that the algorithm is effectively splitting the noise. Once large areas of relatively high and low density have been identified, the main aspect of the data determining whether further splits are productive is the level of noise. So, for example, the perfect line of Figure 6(b) always benefits from further splits, but the noisier pattern of the valley is adequately captured at some point.

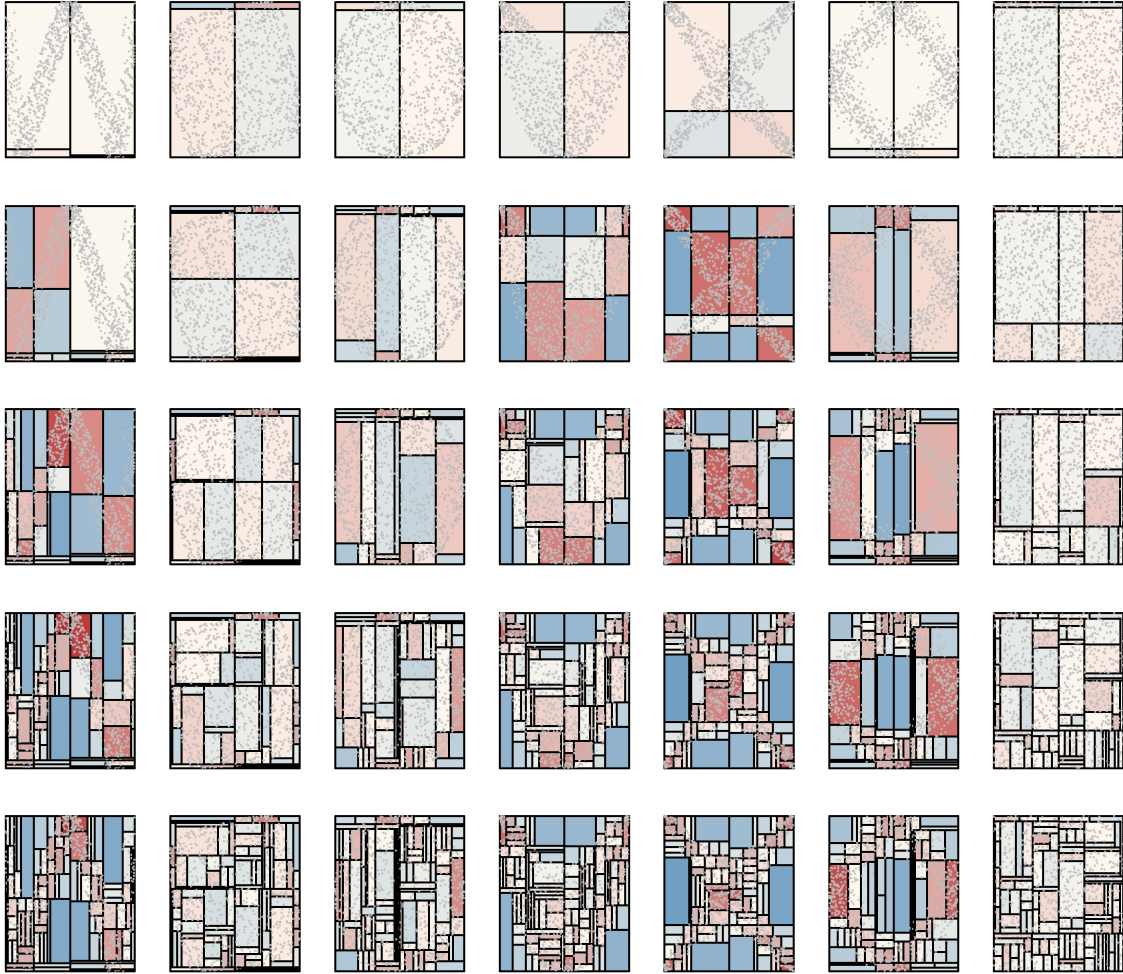


Figure 17: Bins for chi score maximizing splits at increasing depths. By row, depths 2, 4, 6, 8, and 10 are displayed in order. The final bins reflect and summarize the pattern of points given to the algorithm.

Comparing the final row of Figure 17 to randomized binning at a depth of ten in Figure 18, a clear advantage of the maximized binning is better representation of the underlying pattern. Especially for the cross, wave, and valley, random binning produces a larger proportion of thin bins which obscure the pattern of residuals and points. In contrast, maximized binning tends to chase local patterns, leading to many small rectangular bins

around high density areas that provide a sense of the pattern they summarize. Should a visual summary of the data be desired, maximized binning will give more consistent and clear results than random binning.



Figure 18: Bins for random splitting at a depth of 10

## 9 A real data example: S&P 500 returns

For a real data example, consider the S&P 500 constituent data from [Hofert and Oldford \(2018\)](#). The raw data contains a time series of 505 stock prices from the first day of 2007 to the last day of 2009 for stocks included in the S&P 500 index. The goal is to evaluate the pairwise dependence present within the negative log-returns of the 461 stocks with complete records over this period using recursive binning over all  $\binom{461}{2} = 106,030$  pairs. The negative log-return of a stock is the negative logarithm of the ratio in its end-of-day price over two consecutive days, explicitly

$$-\log \frac{S_t}{S_{t-1}}$$

for a stock with value  $S_t$  at time  $t$ . As there are 756 days recorded in the data set, there are 755 log-returns for each stock.

To remove further time dependencies between stock returns day-to-day, the negative log-returns for each stock are fit with an ARMA(1,1)-GARCH(1,1) model and the residuals are taken as a new set of independent pseudo-observations, see details in [Hofert and Oldford \(2018\)](#). The raw data are taken from the `qrmdata` package ([Hofert et al., 2022](#)) and processed by code adapted from the SP500 demo from the `zenplots` package ([Hofert and Oldford, 2020](#)) in order to compute the log-returns and generate the pseudo-observations for recursive binning.

Recursive binning as in Section 8.4 is applied to each of the 106,030 pairs of 755 pseudo-observations to evaluate dependence. Specifically, splitting maximizes the chi score under

the constraint that no bins be created with expected counts less than 5 and splitting is stopped when the expected count in a bin is less than 10, the bin contains no observations, or the depth of the bin is 6. After binning, the  $\chi^2$  statistic is computed over the bins to measure the departure of the observed distribution from that expected under uniformity. Figure 19 displays the resulting statistic values and  $n_{bin}$  for every pair compared to the null quantiles for uniform pairs with 1,000 points from Section 8.2 estimated by quantile regression<sup>14</sup>. Hues from blue to red encode the empirical  $p$ -value of an observed statistic for an S&P 500 pair at a given number of bins in the null data. Partial transparency (alpha-blending) is also used in this plot, but the sheer number of points makes it ineffective at representing the density, so marginal histograms have been added to give a better sense of the location where values are most concentrated.

Most striking in this plot is the significance of nearly every pair. Only 334 of the 106,030 pairs (0.3%) have empirical  $p$ -values less than 0.95, and the  $\chi^2$  statistic values are centred well above the fit null quantiles despite their slightly conservative nature. The pairs generally lie in a single large cluster in  $\chi^2$  statistic and  $n_{bin}$  values and the marginal histograms indicate that within this cluster most points are concentrated in a small region at its center. Only a few dozen pairs lie outside this cluster, including the two very large  $\chi^2$  statistic values for relatively small values of  $n_{bin}$  and the smallest  $\chi^2$  statistic values with the smallest values of  $n_{bin}$ . This suggests that almost every pair in this data set contains some level of dependence, inviting further exploration.

First, consider the exceptionally large statistic values. Figure 20 displays a matrix of the 36 pairs with the largest  $\chi^2$  statistic values in decreasing statistic order from top left to bottom right. For each pair, a scatterplots of the marginal ranks is augmented by a plot of the final binnings coloured by the sign of the Pearson residual (red for positive and blue for negative) and shaded by magnitude. The range of hues is kept constant through all subplots to support direct comparisons between any two binnings.

Immediately apparent in every plot is a strong positive linear relationship between the pairs. Bins along the diagonal line from the bottom left to the top right have more points than expected, while those in the top left and bottom right corners have fewer. Most notably, the bins in the top right and bottom left corners tend to have far more observations than expected. This suggests particularly strong *tail dependence* in these pairs, loosely the probability that large or small values of two random variables occur

---

<sup>14</sup>This choice of null should be somewhat conservative for the case of 755 points. As shown in Figure 12, smaller sample sizes lead to fewer bins and smaller  $\chi^2$  statistic values for the same maximum depth. Therefore, taking the  $\chi^2$  statistic over simulated uniform samples of a slightly larger sample size provides an approximately correct, but slightly conservative, null distribution.



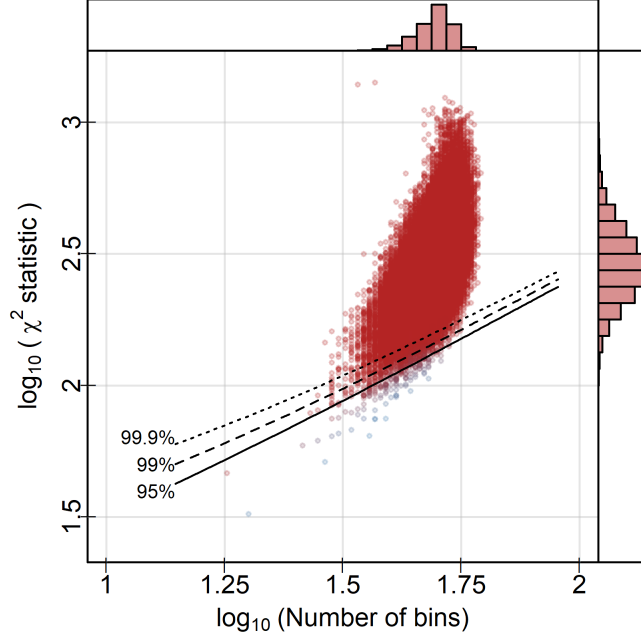


Figure 19: The distribution of  $n_{bin}$  and  $\chi^2$  statistics for the 106,030 S&P 500 pairs split to a maximum depth of 6 compared to some upper quantile estimates of the  $\chi^2$  statistic from  $n_{bin}$  under the null distribution of independence. Most pairs in the S&P 500 data appear to be highly significant.

simultaneously. Precisely, upper tail dependence at  $p \in [0, 1]$  is defined as

$$P(Z_1 > Q_1(p) \mid Z_2 > Q_2(p))$$

and lower tail dependence as

$$P(Z_1 \leq Q_1(p) \mid Z_2 \leq Q_2(p))$$

for random variables  $Z_1, Z_2$  with respective quantile functions  $Q_1(\cdot), Q_2(\cdot)$  (Hofert and Oldford, 2018). As the upper and lower bins approximate these conditional probabilities, albeit for separate quantile values, the shaded residuals in the tails of these plots communicate how much larger the conditional tail probabilities are than would be expected under independence.

Though detecting this tail dependence is not the goal of recursive binning, the most interesting pairs it identifies overlap considerably with the pairs that have the largest upper

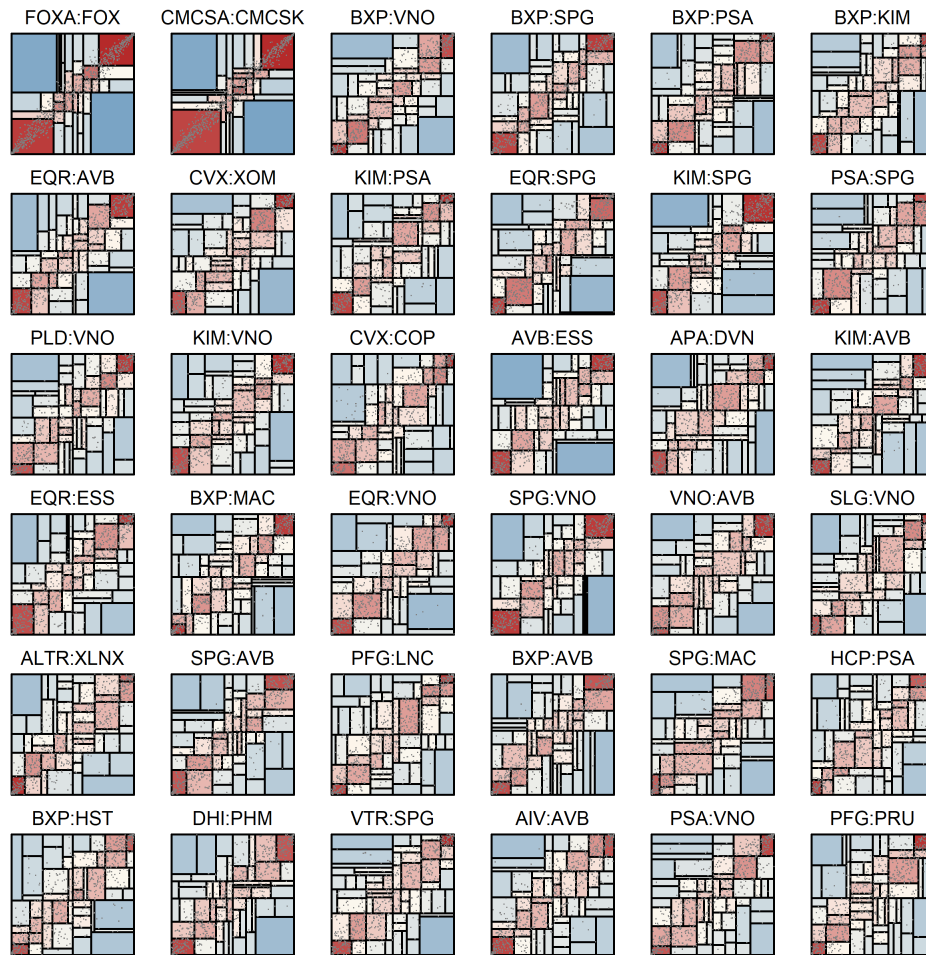


Figure 20: The S&P 500 pairs with the largest  $\chi^2$  statistic values after recursive binning under the splitting and stopping logic described earlier. All pairs show strong linear dependence, especially in the upper and lower tails.

tail dependence. Indeed, 8 the top 10 pairs ranked by upper tail dependence in [Hofert and Oldford \(2018\)](#) can be found in Figure 20. The top two relationships, in particular, correspond to different classes of stock in the same company. This explains not only their strong dependence (especially in the tails), but also their outlying positions in Figure 19 with similarly large  $\chi^2$  statistics for relatively few bins.

At the other end of the spectrum, Figure 21 displays the pairs with the smallest  $\chi^2$

statistic values in decreasing statistic order from top left to bottom right. Residuals are shaded according to the same hues as Figure 20, so a comparison of bins between the two plots is possible. In contrast to the pairs with strong association, the points, bins, and residuals show no obvious patterns for any of these pairs. The magnitude of residuals is generally small and the points show essentially random scatter. It is unsurprising that these pairs are deemed unexceptional by the recursive binning algorithm.



Figure 21: The S&P 500 pairs with the smallest  $\chi^2$  statistic values. These pairs look like realizations of random uniform data, with no strong patterns to the bins, points, or residuals.

Finally consider the pairs with moderate statistic values. Figure 22 displays the 36

pairs with values closest to the median  $\chi^2$  statistic across all 106,030 pairs. Again, the shading is consistent with all previous plots to allow comparisons. These ‘middling’ pairs show relatively weak positive, linear relationships without the strong tail dependence of the pairs with the largest  $\chi^2$  statistic values. Nonetheless, there is a concentration of bins which are shaded faintly red about the main diagonal and others shaded faintly blue in the top left and bottom right corners distinctive of a positive linear relationship. This observation, along with clear separation of statistic values for the simulated data patterns of Section 8.4 from the null distribution, supports the conclusion that the large statistic values across the majority of pairs in the S&P 500 data are not spurious, but instead reflect the power of recursive binning to detect even weak dependence.



Figure 22: S&P 500 pairs with  $\chi^2$  statistic values nearest to the median value. Though the dependence is weak compared to Figure 20, there is still a concentration of bins with more points than expected along the diagonal and bins with fewer points than expected in the off-diagonal corners, suggesting weak positive linear relationships between these pairs.

## 10 Conclusions

This investigation of recursive binning as a method to measure association garners several key observations. First, and perhaps most important, the power of recursive binning to detect association does not appear to depend greatly on whether chi maximizing or randomly placed edges are used to split bins. Both the maximizing splits and the random splits showed pronounced separation of non-null patterns from the null distribution in the simulation study of Section 8.4. Using random splits gives a number of advantages: it is computationally faster, conceptually simpler, and produces a null distribution which is conservatively approximated by the  $\chi^2_{n_{bin}-1}$  distribution if the splitting logic and stop criteria maintain the rule of thumb that the expected count of every bin be  $\geq 5$ . If detecting dependence is the only goal of an investigation, random splits may therefore be preferred to maximizing ones despite, or perhaps because of, their simplicity.

In contrast, maximized score binning produces bins which serve as a superior visual summary of a pairwise relationship. Splits which maximize the chi score, for example, will split off empty sections of a bin and separate regions of particularly high density. The end result is a collection of bins which represent the underlying pattern of points much better than the bins which result from random splits. This comes at a cost of inflated statistic values, requiring modeling or simulation at every application to estimate the significance of an observed statistic value.

In either case, the pattern present in the data impacts the path of the algorithm. For simple linear patterns, dependence can be detected with relatively few splits and bins. More complex patterns may take many splits to detect. For many patterns tested here, it seems a natural depth or resolution is present. Splits below this natural depth may increase the  $\chi^2$  statistic drastically, but after it is reached the statistic grows more slowly at a rate comparable to the null over successive splits.

Recursive binning is a promising method to measure association. It displays high power in the detection of non-linear relationships, can be used to generate a summary visualization of data pairs, and seems to naturally highlight local dependence such as tail dependence in real data. Though the simulations here are not comprehensive, they are highly suggestive of a practical and powerful tool for sorting and summarizing pairwise relationships in large data sets.

## References

- Alan Agresti. Measures of nominal-ordinal association. *Journal of the American Statistical Association*, 76(375):524–529, 1981.
- Francis J. Anscombe. Graphs in statistical analysis. *The American Statistician*, 27(1):17–21, 1973.
- Leo Breiman. Statistical modeling: The two cultures. *Statistical Science*, 16(3):199–231, 2001.
- Leo Breiman and Jerome H. Friedman. Estimating optimal transformations for multiple regression and correlation. *Journal of the American Statistical Association*, 80(391):580–598, 1985.
- Dan Cao, Yuan Chen, Jin Chen, Hongyan Zhang, and Zheming Yuan. An improved algorithm for the maximal information coefficient and its application. *Royal Society Open Science*, 8(2):201424, 2021.
- Daniel B. Carr, Richard J. Littlefield, W.L. Nicholson, and J.S. Littlefield. Scatterplot matrix techniques for large N. *Journal of the American Statistical Association*, 82(398):424–436, 1987.
- Yuan Chen, Ying Zeng, Feng Luo, and Zheming Yuan. A new algorithm to optimize maximal information coefficient. *PLoS One*, 11(6):e0157567, 2016.
- Seung-Seok Choi, Sung-Hyuk Cha, and Charles C. Tappert. A survey of binary similarity and distance measures. *Journal of Systemics, Cybernetics and Informatics*, 8(1):43–48, 2010.
- William G. Cochran. The  $\chi^2$  test of goodness of fit. *The Annals of Mathematical Statistics*, pages 315–345, 1952.
- Jacob Cohen. A coefficient of agreement for nominal scales. *Educational and Psychological Measurement*, 20(1):37–46, 1960.
- Harald Cramér. Remarks on correlation. *Scandinavian Actuarial Journal*, 1924(1):220–240, 1924.
- A. Adam Ding, Jennifer G. Dy, Yi Li, and Yale Chang. A robust-equitable measure for feature ranking and selection. *The Journal of Machine Learning Research*, 18(1):2394–2439, 2017.

- Sebastian Dümcke, Ulrich Mansmann, and Achim Tresch. A novel test for independence derived from an exact distribution of  $i$ th nearest neighbours. *PloS One*, 9(10), 2014.
- Paul Embrechts, Filip Lindskog, and Alexander McNeil. Modelling dependence with copulas. Technical report, ETH Zurich, 2001.
- H. Fairfield Smith. On comparing contingency tables. *The Philippine Statistician*, 6:71–81, 1957.
- Jerome H. Friedman and Werner Stuetzle. John W. Tukey’s work on interactive graphics. *Annals of Statistics*, pages 1629–1639, 2002.
- Salvador Garcia, Julian Luengo, José Antonio Sáez, Victoria Lopez, and Francisco Herrera. A survey of discretization techniques: Taxonomy and empirical analysis in supervised learning. *IEEE transactions on Knowledge and Data Engineering*, 25(4):734–750, 2012.
- Christian Genest and Bruno Rémillard. Test of independence and randomness based on the empirical copula process. *Test*, 13(2):335–369, 2004.
- Leo A. Goodman and William H. Kruskal. *Measures of Association for Cross Classifications*. Springer, 1979.
- Malka Gorfine, Ruth Heller, and Yair Heller. Comment on ”Detecting Novel Associations In Large Data Sets”. *Science*, pages 1–6, 2012.
- Arthur Gretton, Kenji Fukumizu, Choon Teo, Le Song, Bernhard Schölkopf, and Alex Smola. A kernel statistical test of independence. *Advances in Neural Information Processing Systems*, 20, 2007.
- Anders Hald. *A History of Mathematical Statistics from 1750 to 1930*. Wiley, 1998.
- Ruth Heller, Yair Heller, and Malka Gorfine. A consistent multivariate test of association based on ranks of distances. *Biometrika*, 100(2):503–510, 2013.
- Ruth Heller, Yair Heller, Shachar Kaufman, Barak Brill, and Malka Gorfine. Consistent distribution-free k-sample and independence tests for univariate random variables. *The Journal of Machine Learning Research*, 17(1):978–1031, 2016.
- Wassily Hoeffding. A non-parametric test of independence. *The Annals of Mathematical Statistics*, pages 546–557, 1948.



- Marius Hofert and R. Wayne Oldford. Visualizing dependence in high-dimensional data: An application to S&P 500 constituent data. *Econometrics and Statistics*, 8:161–183, 2018.
- Marius Hofert and R. Wayne Oldford. Zigzag expanded navigation plots in R: The R package zenplots. *Journal of Statistical Software*, 95(1):1–44, 2020.
- Marius Hofert, Kurt Hornik, and Alexander J. McNeil. *qrmdata: Data Sets for Quantitative Risk Management Practice*, 2022. URL <https://CRAN.R-project.org/package=qrmdata>. R package version 2022-05-31-1.
- Bo Jiang and Jun S. Liu. Sliced inverse regression with variable selection and interaction detection. *arXiv preprint arXiv:1304.4056*, 652:17, 2013.
- Bo Jiang, Chao Ye, and Jun S. Liu. Nonparametric k-sample tests via dynamic slicing. *Journal of the American Statistical Association*, 110(510):642–653, 2015.
- Harry Khamis. Measures of association: How to choose? *Journal of Diagnostic Medical Sonography*, 24(3):155–162, 2008.
- Justin B. Kinney and Gurinder S. Atwal. Equitability, mutual information, and the maximal information coefficient. *Proceedings of the National Academy of Sciences*, 111(9):3354–3359, 2014a.
- Justin B. Kinney and Gurinder S. Atwal. Reply to Reshef et al.: Falsifiability or bust. *Proceedings of the National Academy of Sciences*, 111(33):E3364–E3364, 2014b.
- Roger Koenker. *quantreg: Quantile Regression*, 2023. URL <https://cran.r-project.org/web/package=quantreg>. R package version 5.97.
- Seung-Chun Lee and Moon Yul Huh. A measure of association for complex data. *Computational statistics & data analysis*, 44(1-2):211–222, 2003.
- Albert M. Liebtrau. *Measures of association*. Sage, 1983.
- Ying Liu, Victor de la Pena, and Tian Zheng. Kernel-based measures of association. *WIREs Computational Statistics*, 10(2), 2018.
- David Lopez-Paz, Philipp Hennig, and Bernhard Schölkopf. The randomized dependence coefficient. *arXiv preprint arXiv:1304.7717*, 2013.

- Tamás F. Móri and Gábor J. Székely. Four simple axioms of dependence measures. *Metrika*, 82(1):1–16, 2019.
- Michael A Newton. Introducing the discussion paper by Székely and Rizzo. *The Annals of Applied Statistics*, 3(4):1233–1235, 2009.
- Karl Pearson. On the criterion that a given system of deviations from the probable in the case of a correlated system of variables is such that it can be reasonably supposed to have arisen from random sampling. *The London, Edinburgh, and Dublin Philosophical Magazine and Journal of Science*, 50(302):157–175, 1900.
- Robin L. Plackett. Karl Pearson and the chi-squared test. *International Statistical Review*, pages 59–72, 1983.
- Adam Rahman. *Preserving measures structure during generation and reduction of multivariate point configurations*. PhD thesis, University of Waterloo, 2018. URL <http://hdl.handle.net/10012/13365>.
- Matthew Reimherr and Dan L. Nicolae. On quantifying dependence: a framework for developing interpretable measures. *Statistical Science*, 28(1):116–130, 2013.
- Alfréd Rényi. On measures of dependence. *Acta Mathematica Academiae Scientiarum Hungarica*, 10(3-4):441–451, 1959.
- David N. Reshef, Yakir A. Reshef, Hilary K. Finucane, Sharon R. Grossman, Gilean McVean, Peter J. Turnbaugh, Eric S. Lander, Michael Mitzenmacher, and Pardis C. Sabeti. Detecting novel associations in large data sets. *Science*, 334(6062):1518–1524, 2011.
- David N. Reshef, Yakir A. Reshef, Michael Mitzenmacher, and Pardis C. Sabeti. Cleaning up the record on the maximal information coefficient and equitability. *Proceedings of the National Academy of Sciences*, 111(33):E3362–E3363, 2014.
- David N. Reshef, Yakir A. Reshef, Pardis C. Sabeti, and Michael Mitzenmacher. An empirical study of the maximal and total information coefficients and leading measures of dependence. *The Annals of Applied Statistics*, 12(1):123–155, 2018.
- Berthold Schweizer and Edward F. Wolff. On nonparametric measures of dependence for random variables. *Annals of Statistics*, 9(4):879–885, 1981.
- David W. Scott. A note on choice of bivariate histogram bin shape. *Journal of Official Statistics*, 4(1):47, 1988.

- Claude E. Shannon. A mathematical theory of communication. *The Bell System Technical Journal*, 27(3):379–423, 1948.
- Karl Friedrich Siburg and Pavel A. Stoimenov. A measure of mutual complete dependence. *Metrika*, 71(2):239–251, 2010.
- S.D. Silvey. On a measure of association. *The Annals of Mathematical Statistics*, pages 1157–1166, 1964.
- Noah Simon and Robert Tibshirani. Comment on ”Detecting Novel Associations In Large Data Sets” by Reshef et al., Science dec 16, 2011. *arXiv preprint arXiv:1401.7645*, 2014.
- Abe Sklar. Random variables, distribution functions, and copulas: a personal look backward and forward. *Institute of Mathematical Statistics Lecture Notes – Monograph Series*, pages 1–14, 1996.
- Michael A. Stephens. Edf statistics for goodness of fit and some comparisons. *Journal of the American Statistical Association*, 69(347):730–737, 1974.
- Stephen M Stigler. Francis Galton’s account of the invention of correlation. *Statistical Science*, pages 73–79, 1989.
- Gábor J Székely and Maria L. Rizzo. Brownian distance covariance. *The Annals of Applied Statistics*, pages 1236–1265, 2009.
- Olivier Thas and Jean-Pierre Ottoy. A nonparametric test for independence based on sample space partitions. *Communications in Statistics-Simulation and Computation*, 33(3):711–728, 2004.
- Dag Tjøstheim, Håkon Otneim, and Bård Støve. Statistical dependence: Beyond pearson’s  $\rho$ . *Statistical science*, 37(1):90–109, 2022.
- Leland Wilkinson and Graham Wills. Scagnostics distributions. *Journal of Computational and Graphical Statistics*, 17(2):473–491, 2008.
- Leland Wilkinson, Anushka Anand, and Robert Grossman. Graph-theoretic scagnostics. In *IEEE Symposium on Information Visualization, 2005. INFOVIS 2005.*, pages 157–164. IEEE, 2005.
- Wenjun Zheng, Dejian Lai, and K. Lance Gould. A simulation study of a class of non-parametric test statistics: a close look of empirical distribution function-based tests. *Communications in Statistics-Simulation and Computation*, pages 1–17, 2021.